# *Investigation of Surface Waves on Hydrodynamic Lubrication*

By

George Costa

B.S. Mechanical Engineering

University of Massachusetts Dartmouth, 1998

Submitted to the Department of Mechanical Engineering in

Partial Fulfillment of the Requirements for the Degree of

Master of Science in Mechanical Engineering

At the

Massachusetts Institute of Technology

June 2000

© 2000 Massachusetts Institute of Technology

All Rights Reserved

Signature of Author.....

Department of Mechanical Engineering

May 5, 2000

Certified By.....

.....

Douglas P. Hart

Professor of Mechanical Engineering

Thesis Supervisor

Accepted by .....

Professor Ain A.Sonin

Professor of Mechanical Engineering

Chairman, Committee for Graduate Students

MASSACHUSETTS INSTITUTE OF TECHNOLOGY

SEP 2 0 2000

LIBRARIES

ENG

# *Investigation of Surface Waves on Hydrodynamic Lubrication*

By:
George Costa

Submitted to the Department of Mechanical Engineering in
Partial Fulfillment of the Requirements for the Degree of
Master of Science in Mechanical Engineering

**Abstract**

An experimental and theoretical investigation was carried out on mechanical face seals to evaluate the effects of surface wave geometry on hydrodynamic lubrication performance. It was found theoretically that there lies an optimum surface wave height to generate maximum hydrodynamic load support. In addition it was found theoretically that increasing the surface wave amplitude and increasing the number of waves present on a face seal act to stiffen the seal resisting deflections at the surface.

Experimentally it was demonstrated the effectiveness of using *Laser Induced Fluorescence (LIF)* to visualize surface wave deflections and pressure induced leakage present on a mechanical face seal. Correlation of LIF surface deflection experiments to Hertzian contact deflections was successful. Experiments showed that surface wave deflections are proportional to the load applied to the seal for a given load range of 0 to 600 N.

**Thesis Supervisor: Douglas P. Hart**
**Professor of Mechanical Engineering**

**Acknowledgements**

I would like to thank the Mechanical Engineering Department at the Massachusetts Institute of Technology for providing the opportunity to purse my graduate education. I am honored to have been accepted and to have experienced all that MIT has to offer.

I would like to thank Steve Aoyama would served as an engineering mentor for three years during my employment in Research and Development at Titleist and FootJoy Worldwide. I greatly appreciate all of the guidance and knowledge he provided.

I would like to thank the entire Mechanical Engineering faculty and staff at the University of Massachusetts Dartmouth. Without their dedication and perseverance I would not be the engineer I am today. In particular, I would like to thank Dr. Raymond Laoulache, who throughout the years has served as an excellent mentor and friend. His dedication to engineering education is unparalleled and I appreciate everything he has done to help me become a better engineer.

I would like to thank Caterpillar, Incorporated for providing the financial and technical support for my Masters Degree. In particular, I would like to thank Mark "the Weasel" Kiesel and Kristy Johnson for all of their work to assist me in reaching my goals. Without them this work would have been impossible.

I would like to thank my colleagues in the Fluid Mechanics Lab who made my time at most enjoyable. In particular, I would like to thank Micah D. Smith and Carlos Hidrovo Chavez. Micah provided the lab entertainment while Carlos provided a wealth of information and opinions (some of which resulted in arguments which lasted for days). I appreciate his stubbornness because he forced me to really think through and understand many of the details of my research.

I would like to thank Michaela Schermer who was there for me when I really needed it. Her love and support is something I will cherish for a lifetime. She has made this past year wonderful and I look forward to the years ahead. Ich liebe Dich, mein Schatzi.

Finally I would like to thank my parents, Jose and Margarida Costa, whose discipline and care has enabled me to acheive my goals. The most important thing I learned from them is the value and benefit of hard work. To them I dedicate this thesis. My accomplishments are because of their hard work.

## Table of Contents

1. Introduction and Background....8
   1.1 Problem Statement....9
   1.2 Previous Research....11
   1.3 Thesis Research....13

2. Theoretical Modeling....14
   2.1 Hertzian Contact Model for Wavy Surfaces....14
   2.1a Numerical Study of Wavy Surface Deflections....17
   2.2 Hydrodynamic Model of Wavy Surfaces....19
   2.2a Derivation of Hydrodynamic Model From *Navier Stokes*....20
   2.2b Lubrication Modeling Using Reynolds Equation....21
   2.2c Numerical Study of Wavy Surfaces Using Reynolds Equation....24
   2.3 Surface Tension Model for Face Seals....28

3. Experimental Setup....30
   3.1 Test Parameters....31
   3.2 Visualizing Oil Film Thickness....33
   3.3 Principles of *Laser Induced Fluorescence*....33
   3.3a Laser and Optical Measurement Setup....33
   3.4 Seal Geometry Measurements....36
   3.4a Measurement of Free Surface Wave Geometry....36

4. Experimental Results....38
   4.1 LIF Wave Deflection versus Load....38
   4.2 Wave Amplitude Experiment....42
   4.3 Internally Pressurized Leakage Experiment....48

5. Discussion....53
   5.1 Surface Wave Deflections....53
   5.2 Surface Wave Lubrication....54
   5.3 Internal Pressurization....57

6. Conclusions....58

7 Future Work....60

References....63

Appendix A Description of Programs Written for Anaylsis....65

Appendix B Dyed Oil Preparation for Laser Induced Fluorescence Experiments....83

**List of Figures**

1. Cross Section View of Seal Schematic.....8
2. Metal Face Seal Used for Analysis.....8
3. Example Observation of Cavitation.....12
4. Example LIF Image.....13
5. Original Seal Surface Wave Geometry.....15
6. Deflected Seal Surface Wave Geometry.....15
7. Correlation of Contact Patch to Wave Height. .....16
8. Effect of Number of Waves.....17
9. Effect of Wave Height.....17
10. Normalized effect of Number of Waves .....18
11. Normalized effect of Wave Height.....18
12. Theoretical Friction Coefficient versus Sommerfeld Number.....22
13. Example Pressure Solution.....24
14. Example Seal Geometry.....24
15. Effect of Number of Waves on Load Support.....25
16. Effect of Number of Waves on Coefficient of Friction.....25
17. Effect of Wave Height on Load Support.....26
18. Effect of Wave Height on Friction.....26
19. Effect of Minimum Film Thickness on Load Support.....27
20. Theoretical Friction Coefficient versus Sommerfeld Number.....27
21. Schematic of Surface Tension Problem.....28
22. Surface Tension Gap Height versus Internal Pressure.....29
23. Cross-Section of Experimental Test Rig.....30
24. Button Load Cell.....30
25. Load Cell Used for Torque Measurement.....30
26. Face Seal Experimental Test Rig.....31
27. Slip Ring Assembly.....32
28. Thermocouple Locations on a Seal Cross-Section.....32
29. Example LIF Image.....33
30. Example Intensity Plot.....33
31. Operational Principle of LIF.....34

**List of Figures**

32. Beam Expanding Optics Principle.....34
33. New Wave Pulsed Nd-YAG 532nm Laser Beam Profile.....35
34. Intensity Plots of Laser Beam Profile.....35
35. Example of a Typical High Accuracy Brown and Sharpe CMM.....37
36. Waviness Symbols Plots.....38
37. Seal Waviness Plots.....38
38. Etched Numeric Pattern.....39
39. Typical LIF Image Captured.....39
40. LIF Experimental Load Results.....39
41. Experimental Result at 15 lbf Loading.....40
42. Actual Unloaded Surface Geometry.....40
43. LIF Load Deflection Results.....40
44. Experimental and Theoretical Results of Wave Deflection.....41
45. Test Seal A Wave Geometry.....42
46. Test Seal B Wave Geometry.....42
47. f-G Plot for Test Seal A at 600 N.....43
48. f-G Plot for Test Seal B at 600 N.....43
49. Experimental versus Theoretical f-G Plot for Test Seal B at 600 N.....44
50. f-G Plot for Test Seal A at 120 N.....45
51. f-G Plot for Test Seal B at 120 N.....45
52. Experimental versus Theoretical f-G Plot for Test Seal A at 120 N.....46
53. Experimental versus Theoretical f-G Plot for Test Seal B at 120 N.....46
54. Effect of Load to f-G Plot and Experimental Fit.....47
55. Leakage Test Surface Wave Geometry.....48
56. Description of LIF Leakage Images.....49
57. Pressure Test at 5 kPa.....49
58. Pressure Test at 40 kPa.....49
59. Pressure Test at 60 kPa.....49
60. Pressure Test at 5 kPa.....49
61. Pressure versus Time Relationship at 35 Degrees Location..... 50

**List of Figures**

62-65. 140 Second Internal Pressure Test with Leakage at 320 Degree Location……51

66. Pressure versus Time Relationship at 320 Degree Location….. ……..52

67. Non-Laser Engraved Seal Temperature Results……..56

68. Laser Engraved Seal Temperature Results……..……56

69. Contact Angle Illustration……57

# Chapter 1
# Introduction

In many applications, the wear of two sliding surfaces can be minimized via careful lubrication. The fundamental goal of sliding plate lubrication is to promote hydrodynamic lift, thereby reducing friction and minimizing wear. Hydrodynamic lift can best be produced if the surfaces are specifically engineered to generate lift. This has been a goal of tribologists for some time and several researchers such as Lebeck and Young [1], and Etsion [2] have contributed greatly to knowledge in this field. However, despite extensive research, there still lacks a fundamental understanding of the geometric parameters responsible for the generation of hydrodynamic lubrication in the sliding plate application. This is the thrust of the work described in this document.

This thesis will investigate sliding plate lubrication, more specifically, the potential for generation of hydrodynamic lift, by looking closely at one particular application – the metal face seal. Metal face seals, also commonly known as metal-to-metal seals, are used extensively in such applications as final drives, rotating housings, and other lubricated joints. Industries that commonly use metal face seals include construction and mining, power generation, processing industries, transportation, agriculture, and aerospace. The purpose of the metal face seals in each of these applications is generally to keep two internal fluids from mixing or to prevent leakage of a vehicle's internal lubricating fluid while preventing debris from entering a tribological system. The metal-to-metal interface of a metal face seal is preferred to an elastomeric sealing system when exposed to harsh and extreme conditions, such as high temperature, high sliding speed, or high debris concentration.

In 1988, mechanical face seal product sales totaled more than 300 million dollars [3], not including the cost of downtime and repair. In order to prevent downtime and eliminate the need for costly vehicle repairs due to the untimely failure of these seals, a fundamental understanding of the mechanisms responsible for lubrication generation is necessary. With intimate knowledge of the metal face seal, designers can hope to reduce initial cost, increase performance, and extend seal life, thus reducing additional costs associated with downtime and repair.

Figure 1 shows the configuration of the metal face seal pair investigated in this work. Figure 2 shows the actual sealing face of one half of the seal set represented in Figure 1.

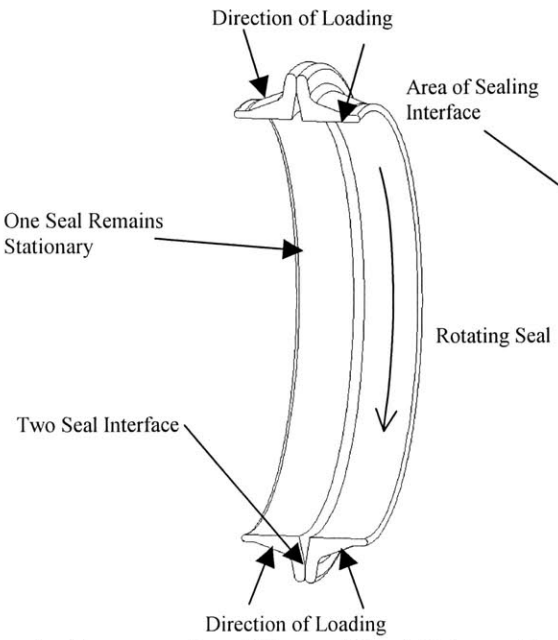


Figure 1. Cross section View of Seal Schematic

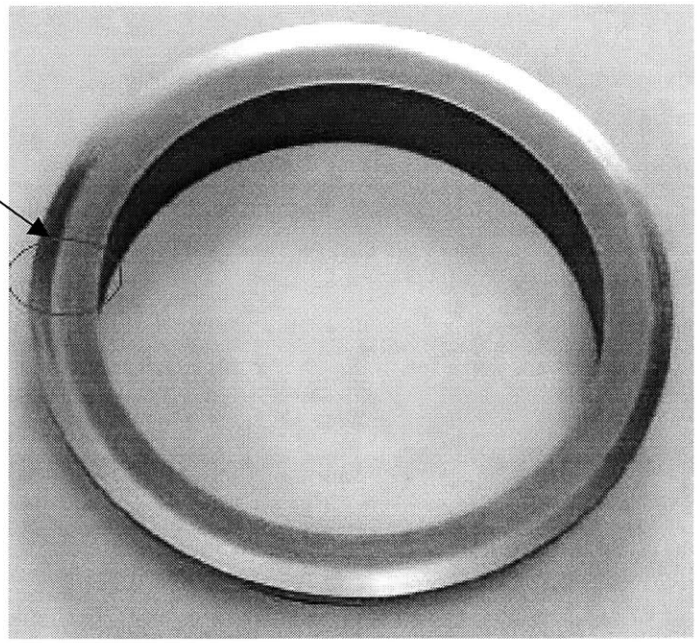

Figure 2. Metal Face Seal Used for Analysis

## 1.1 Problem Statement

It is known that surface features located at the sealing interface will produce hydrodynamic load support (Lebeck [4], Etsion [2]). Features that are believed to induce lift are:

- Macro Geometry in the form of Surface Waves
- Macro Geometry in the form of Radial Taper
- Micro Geometry in the form of Surface Roughness

The focus of this thesis is on the geometry of surface wave features their effect on mechanical face seal performance. This will be investigated through theoretical and experimental studies.

The first area of study involves the deflection of the surface wave under load. Hertzian contact mechanics will be used to help predict the theoretical deflections of the surface wave under load. This will be accomplished experimentally by using the novel visualization technique of *Laser Induced Fluorescence*, where the geometry of the mechanical face seal will be extracted under a series of different loadings.

The second area of study will involve the geometry of a surface wave and its influence on hydrodynamic lubrication. A model based on the Reynolds equation has

been developed and theoretically investigated to predict hydrodynamic load support. Experimentally, this will be evaluated using mechanical face seals of varying wave heights.

The final area of study will involve the geometry of a surface wave and its influence on leakage when pressurized internally. A model based on surface tension has been developed which relates the gap height between the surface wave and the secondary mating surface to the required internal pressure to initiate leakage. Experimentally, this will be evaluated using *Laser Induced Fluorescence*, to observe leakage as the internal pressure is increased.

Referring to Figure 2, a surface wave is a circumferential variation in height on the sealing interface, e.g. the highly polished region on the outer diameter of the seal. Surface waves are a consequence of the manufacturing methods used. Many different processes contribute to the overall waviness. These processes may involve initial casting warp, unsymmetrical loading during a material removal process, inhomogeneous materials, or a non-uniform temperature distribution during a material removal process.

In the present work, the surface wave is measured in the unloaded free state. Chapter 2.1 deals with the geometry of a wave under static loading conditions. A Hertzian model has been established in order to predict wave deflection given a certain load.

Knowledge of surface waviness information is important in the determination of hydrodynamic load support. Hydrodynamic load support is achieved when fluid imparts onto the wave, creating a net positive pressure, and acts to separate the two surfaces. Hydrodynamic load support is the sole load support mechanism before the minimum film thickness approaches zero, thus making it necessary to predict the deformed wave geometry *a priori*. In the case where the minimum film thickness is equal to zero, Boundary lubrication is predominant and the case should be dealt with accordingly. boundary lubrication requires knowledge of the asperity interactions in order to predict face seal behavior during operation.

Chapter 2.2 includes a derivation of the governing lubrication equations and the solution technique used to calculate load support, friction coefficient, and Sommerfeld number (a dimensionless parameter which describes lubrication). These results will be compared to experimental data in Chapter 4.2. An extensive comparison will be conducted in order to determine the accuracy of the hydrodynamic lubrication model. Obtaining a solution will require knowledge of the deformed geometry and an iteration scheme to converge downward toward a minimum film thickness. Once the solution for

the pressure distribution is known, coefficient of friction and Sommerfeld number can be calculated, making the state of lubrication evident.

Another requirement of the face seal is that there not be excessive leakage. A model has been developed which takes into consideration the gap between two surfaces and the required pressure to overcome surface tension forces. This model is presented in detail in Chapter 2.3 and experimental results are presented in Chapter 4.3. This final analysis provides a check against the initial modeling to make sure that any design change does not allow the possibility for leakage.

Experiments that were conducted to evaluate face seal performance utilized various data acquisition techniques, primarily *Laser Induced Fluorescence* (LIF) and traditional (speed, torque, and temperature) measurements. *Laser Induced Fluorescence* (LIF) was used to extract qualitative information pertaining to film thickness and leakage. This experimental technique will be covered in detail in Chapter 3.3

The final objective of the research is to compile both theoretical and experimental results and use them to create a surface wave design methodology for face seals. This allows seal design engineers to follow guidelines when selecting and or designing such components from a lubrication point of view. All models presented herein should be taken in context with their assumptions.

## 1.2 Previous Research

Alan O. Lebeck has made a significant contribution to mechanical face seal research. He holds numerous patents on wavy face seal designs [5, 6]. In conjunction with Lionel Young, Lebeck developed a design of a moving wave mechanical face seal [8]. This design involves using gas pressure imparted onto specific locations of a seal cross section. This pressure creates moments about the seal ring cross-section, inducing waviness. The moving wave is developed over time by increasing pressure to compensate for mechanical wear. Seals using this design exhibited low coefficient of friction values while maintaining negligible amounts of leakage.

Other investigators such as Etsion and Kligerman [9] and Etsion and Burstein [10] have also pursued other geometric surface features that promote hydrodynamic lubrication. They do not utilize the concept of surface waves but instead deal with micro-pores embedded into the sealing surface. These pores resemble dimples of a golf ball and have been optimized for hydrodynamic load support. Theoretical modeling of these pores has led to consistent results and correlates to theory.

Green and Insolia [11] have investigated issues concerning mechanical face seal dynamics. They have developed a commercial software package *Seal Design System, SDS*, which solves for dynamic motion caused by hydrodynamic load support. Their contribution to face seal research is the coupling of dynamics to the hydrodynamic lubrication, this had not been previously attempted. Their approach is unique in the sense that all components of the face seal assembly are considered. Therefore, evaluation of new seal designs, loading mechanisms, and lubricants are easily performed.The software is capable of providing real time visualization of the seal rotor and associated components. Dynamic rotor instabilities have been shown to cause excessive leakage and seal failure. The program allows seal designers to quickly evaluate the influence of each component in a seal assembly.

Nau [12] has reported observations of film cavitation in face seals. An example of his observations can be found in Figure 3. His experiments involve using a metal face seal rotating against a glass plate to enable flow visualization. Imaging of the cavitation region was possible using floodlights for illumination and a conventional camera system with a 1/100 second exposure time. Nau demonstrated how cavitation could occur due to the creation of divergent flow sections. These divergent flow sections were created by angular misalignment of the seal and also by loading of the glass plate in order to produce bending across the seal interface. Cavitation was evident across a wide range of operating conditions. Nau showed that at high surface speeds and high loadings, cavitation was most predominate. However the implications of this phenomena were not addressed. Nau comments that cavities observed are comprised of air bubbles entrapped in the liquid and differs from the vapor bubbles which are responsible for erosion of marine propeller blades. Many investigators incorporate cavitation conditions in their theoretical modeling although none have actually addressed the significance of implementing these conditions.

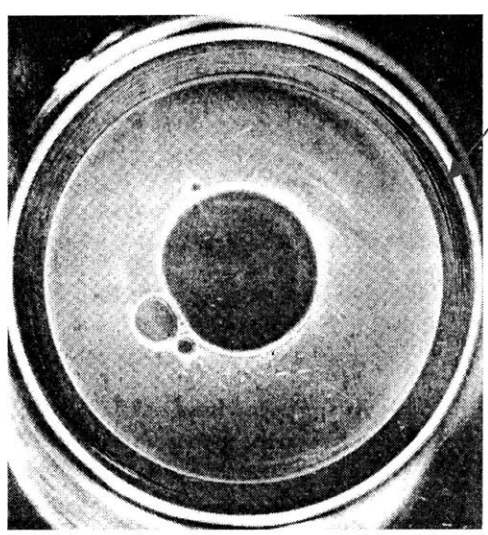


Figure 3. Example Observation of Cavitation by Nau [12]

## 1.3 Thesis Research

The goal of this research is to understand the importance of surface waves on lubrication. Experiments reported herein utilize the novel technique of fluid flow visualization via *Laser Induced Fluorescence* (LIF). LIF allows a non-intrusive method of capturing 3-D information of oil presence. This information is beneficial in extracting oil film thickness and seal leakage. Film thickness information is proportional to light intensity levels imaged by a digital camera. An Example of LIF can be seen in Figure 4.

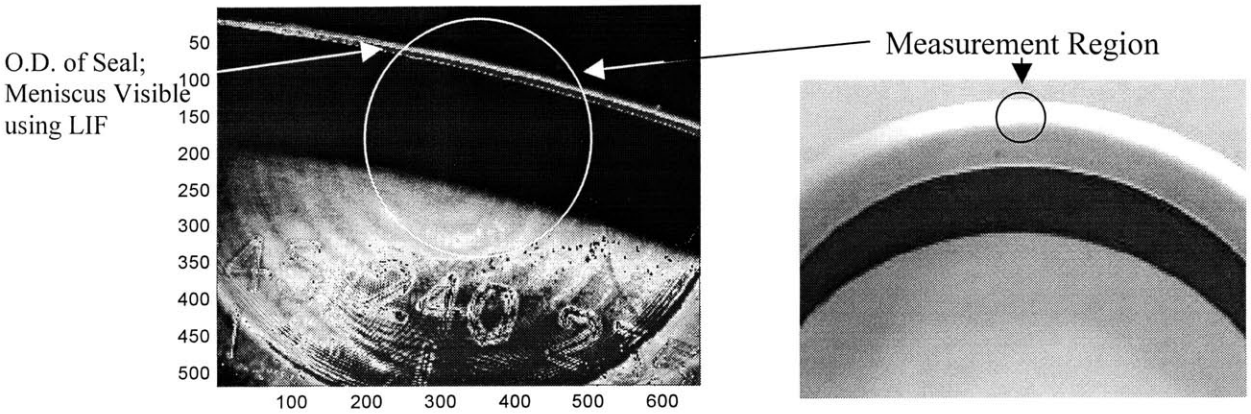


Figure 4. Example of LIF Image.

Images collected may be formatted and condensed in movies, which allows rapid evaluation of long duration experiments. Research to be presented combines the use of LIF and traditional sensor methods to describe operational characteristics of a metal face seal. In particular, issues concerning seal deflections at the interface, long-term lubrication behavior and leakage of the sealing junction were studied. Previous investigators have neglected the use of such techniques to describe such tribiological interactions.

# Chapter 2

# Theoretical Modeling

Three theoretical models have been developed to describe the behavior of mechanical face seals. The purpose of modeling is to provide a method of predicting certain behavior associated with the lubrication mechanisms. To aid in the analysis of the models, several programs were developed using the Student Edition of MatLab v5.3. All programs developed have a Windows style graphical interface and have been tested under Windows NT on a 450MHz Pentium III computer with 512MB RAM. Program descriptions have been provided in Appendix A.

## 2.1 Hertzian Contact Model for Wavy Surfaces

In this case, the concern is the overall deflection of each wave of a given face seal geometry. This information will be used to help predict the overall hydrodynamic lift support in Section 2.2. The method of solution is the closed form of the Hertz theory of line contact (Johnson [13]) applied to a wavy surface. A brief overview of key issues will be presented herein. Appendix A contains the program descriptions of *hertz.m* and *hertztheory.m,* which were used to generate the solutions to the contact mechanics problem. Referencing Figure 5 and Figure 6, the associated nomenclature is as follows:

$\lambda$ (m); Wavelength of one wave

$\Delta$ ($\mu$m); Amplitude of one wave

2a (m); Contact width of deflected wave

2b (m); Undeflected portion of the wave under load

h (m); Amount of wave deflected

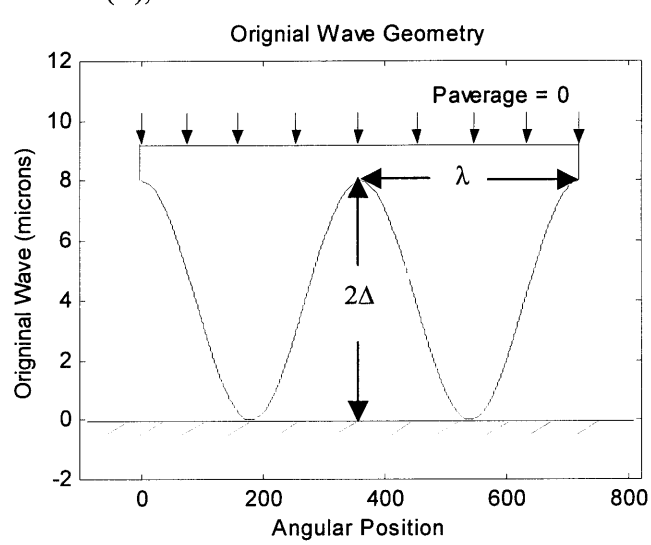


Figure 5. Original Seal Surface Wave Geometry

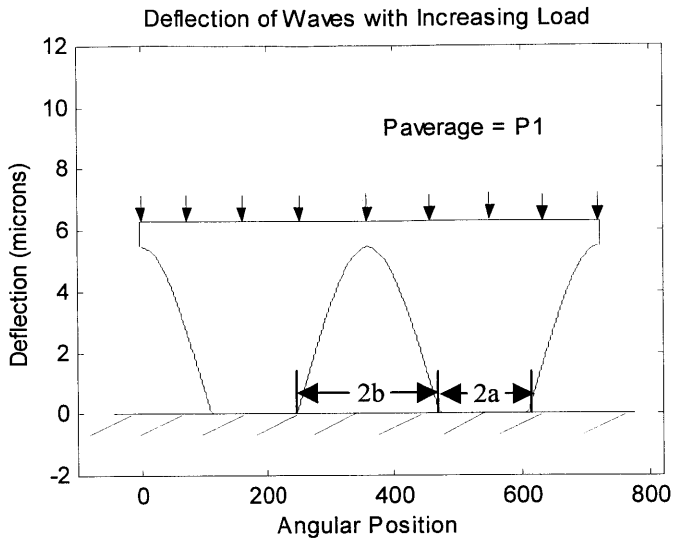


Figure 6. Deflected Seal Surface Wave Geometry

The Hertz closed form solution for two-dimensional contact between cylindrical bodies will be used. In this case, one radius is considered to be infinite and the problem reduces to line contact of a cylinder and a plate, Johnson [13].

$$a^2 = \frac{4PR}{\pi E^*} \qquad \text{Eq.(1)}$$

$$P = P_1\lambda \text{ (N/m)}$$

$$1/R = \text{Radius of Curvature}$$

$$\text{Radius of Curvature for a Wave} = \frac{4\pi^2\Delta}{\lambda^2}$$

Where

$$E^* = \left[\frac{(1-\nu_1)^2}{E_1} + \frac{(1-\nu_2)^2}{E_2}\right]^{-1} \qquad \text{Eq.(2)}$$

And

$E^*$ (N/m$^2$); Effective Modulus of the two materials

$E_1$= Primary Material Modulus

$E_2$= Secondary Material Modulus

$\nu_1$= Primary Material Poisson Ratio

$\nu_2$= Secondary Material Poisson Ratio

Assumptions:

- Material that is not in contact does not deform.
- The material with the infinite radius also has infinite stiffness.
- Values of deflection are valid for ratios of real/apparent area (2a/λ) of contact up to λ/2.
- Deflections are small so as to adhere to elastic stress/strain theory.
- Solution must be modified for multiple waves.

Equation (1) provides the deflected contact patch given a load/length, P. Correlating this deflected contact patch to vertical displacement, we obtain:

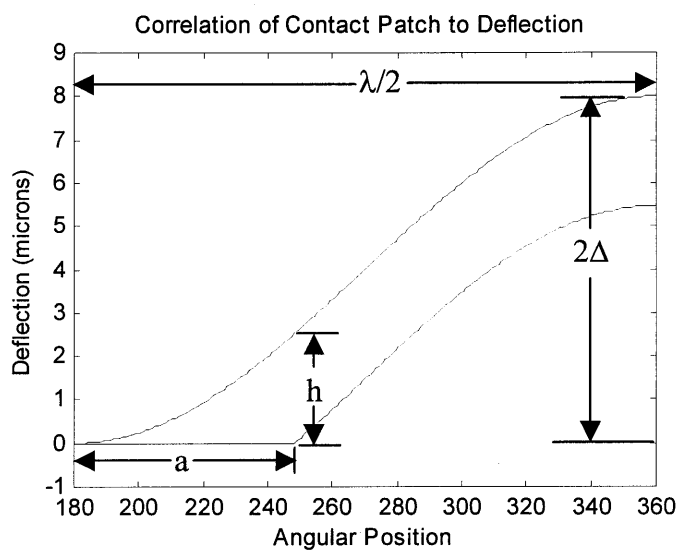


Figure 7. Correlation of Contact Patch to Wave Height.

$$h = \Delta Cos(\theta + 180) + \Delta$$

Where:

$$\theta = \frac{180}{\lambda/2} a$$

If the average pressure distribution is known, the solution becomes:

$$h = \Delta Cos\left[2\sqrt{\frac{P_1 \lambda}{\pi \Delta E^*}} + \pi\right] + \Delta$$

To use normal load as an input:

$$\frac{P_2}{bN} = P_1 \lambda$$

Where:

b = Face seal width (m)

N = Number of load supporting wave crests

$$h = \Delta Cos\left[2\sqrt{\frac{P_2}{bN\pi\Delta E^*}} + \pi\right] + \Delta \qquad \text{Eq.(3)}$$

Equation 3 provides the deflections given a load and geometry as input. The output of Equation 3 will be a cosine wave shifted downward by a value, *h*. This results in negative values of wave geometry that correspond to contact locations. To correct for this, the negative values should be located and set to zero. Results obtained are of the form shown in Figures 5 and 6.

### 2.1a Numerical Study of Wavy Surface Deflections

From the Hertzian contact model, the influence of wave amplitude and number of waves on surface deflections can be investigated. Values for this theoretical study were selected based on the realistic geometry, operating conditions, and material properties of the face seal experiments discussed in Chapter 4.1.

Using:

| | |
|---|---|
| $E_1$= 200 Gpa (Steel) | $E_2$= 72 Gpa (Quartz) |
| $\nu_1$= 0.33 | $\nu_2$= 0.17 |
| Seal Diameter = 192 mm | Face Width = 2 mm |
| Load Range = 0-1000 N | |

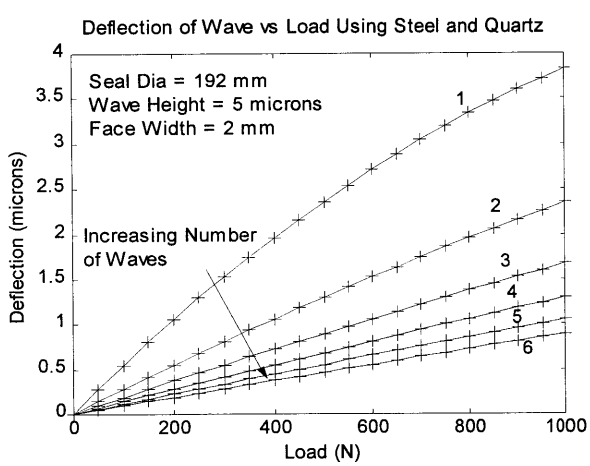


Figure 8. Effect of Number of Waves

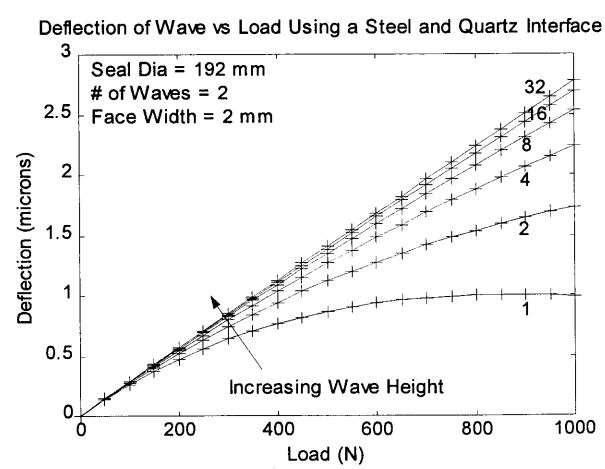


Figure 9. Effect of Wave Height

It can be seen from Figure 8 that if the number of waves on a seal of a given diameter increases, the overall deflection is greatly decreased. Increasing the number of waves present on a seal is analogous to shortening the length of a beam in pure bending. Each wave crest contributes to equally support the applied load. Therefore, stiffening the seal (or beam) is accomplished by increasing the number of supporting wave crests. This can be seen by closer inspection of Equation 3. As $N$ becomes large in relation to $P$, then $h$ approaches zero.

$$h = \Delta Cos\left[2\sqrt{\frac{P_2}{bN\pi\Delta E^*}} + \pi\right] + \Delta \qquad \text{Eq.(3)}$$

Figure 9 demonstrates the effect of increasing the total wave height (peak to valley). For the given load range the effect of increasing wave height does not significantly change for wave heights greater than 16 μm. Because wave amplitude, $\Delta$, is contained in the denominator of the square root term, the same argument that was provided for $N$ applies in this case even though increasing $\Delta$ does not shorten the length of the beam. Instead, it increases the radius of curvature which helps to stiffen the seal (or beam).

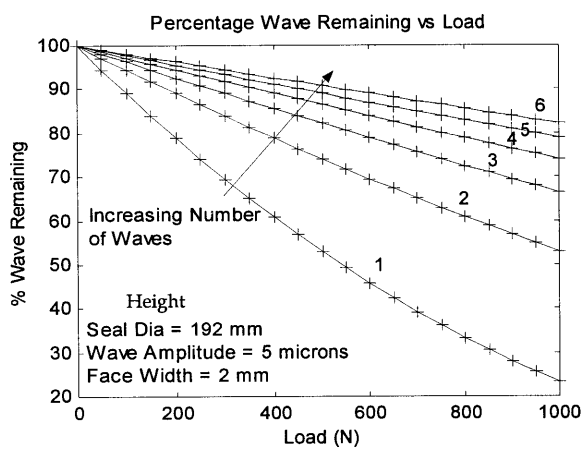


Figure 10. Normalized effect of Number of Waves

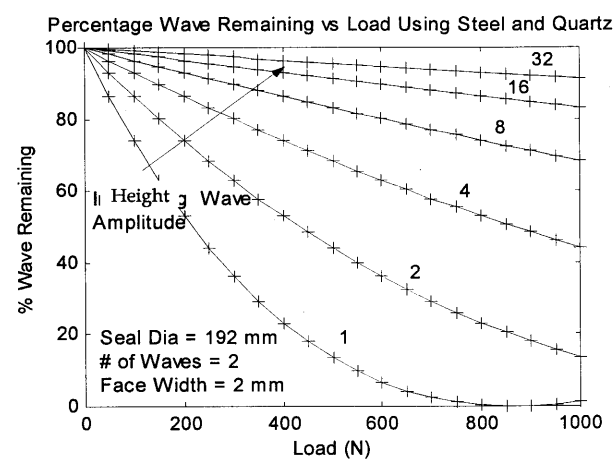


Figure 11. Normalized effect of Wave Height

Figures 10 and 11 are normalized representations of Figures 8 and 9. The data was normalized in order to allow comparison to experimental data. *Laser Induced Fluorescence* was used to extract the surface wave geometry under load. Surface wave deflection data can be represented in a percentage format and will be presented in Chapter 4.1.

## 2.2 Hydrodynamic model of Wavy Surfaces

Under dynamic operation a wavy surface may produce adequate hydrodynamic load support. This is due to a net positive pressure created by converging geometry. Diverging geometries tend to produce negative pressures but are limited by the vapor pressure of the liquid. Once the vapor pressure of the liquid is reached, the phenomenon of cavitation occurs in the face seal, as has been investigated by Nau [12], Lebeck [3], Salant and Payvar [20],and Etsion [10]. In the context of this analysis, cavitation will not be considered. When negative pressures are calculated, they will be set to zero as a first order approximation, known as the Grümbel or half-Sommerfeld condition. This approximation is validated by the necessity for a large pressure in order to support moderate loads. Another means to validate this condition is to use the vapor pressure of the lubricant. Incorporation of the vapor pressure is necessary for very light loading, where max pressure is on the order of a 1-3 atmospheres. Incorporation of cavitation conditions involves the use of more complex numerical methods than these implemented by this author. The programs *Reynolds.m* and *Hydrodynamic.m* were used in the analysis presented herein, and can be found in Appendix A.

### 2.2a Derivation of Hydrodynamic Model From *Navier Stokes*

The following is the well-known *Navier Stokes* Equations in polar coordinates (Acosta [14]):

R direction

$$\frac{\partial v_r}{\partial t}+v_r\frac{\partial v_r}{\partial r}+\frac{v_\theta}{r}\frac{\partial v_r}{\partial \theta}+v_z\frac{\partial v_r}{\partial z}-\frac{v_\theta^2}{r}=-\frac{1}{\rho}\frac{\partial p}{\partial r}+\frac{1}{3}\frac{\mu}{\rho}\frac{\partial \Theta}{\partial r}+\frac{\mu}{\rho}\left[\frac{1}{r}\frac{\partial}{\partial r}\left(r\frac{\partial v_r}{\partial r}\right)+\frac{1}{r^2}\frac{\partial^2 v_r}{\partial \theta^2}+\frac{\partial^2 v_r}{\partial z^2}-\frac{v_r}{r^2}-\frac{2}{r^2}\frac{\partial v_\theta}{\partial \theta}\right]+f_r \quad \text{Eq.(4)}$$

θ direction

$$\frac{\partial v_\theta}{\partial t}+v_r\frac{\partial v_\theta}{\partial r}+\frac{v_\theta}{r}\frac{\partial v_\theta}{\partial \theta}+v_z\frac{\partial v_\theta}{\partial z}-\frac{v_r v_\theta}{r}=-\frac{1}{\rho}\frac{1}{r}\frac{\partial p}{\partial r}+\frac{1}{3}\frac{\mu}{\rho}\frac{1}{r}\frac{\partial \Theta}{\partial \theta}+\frac{\mu}{\rho}\left[\frac{1}{r}\frac{\partial}{\partial r}\left(r\frac{\partial v_\theta}{\partial r}\right)+\frac{1}{r^2}\frac{\partial^2 v_\theta}{\partial \theta^2}+\frac{\partial^2 v_\theta}{\partial z^2}-\frac{v_\theta}{r^2}-\frac{2}{r^2}\frac{\partial v_r}{\partial \theta}\right]+f_\vartheta \quad \text{Eq.(5)}$$

Z direction

$$\frac{\partial v_z}{\partial t}+v_r\frac{\partial v_z}{\partial r}+\frac{v_\theta}{r}\frac{\partial v_z}{\partial \theta}+v_z\frac{\partial v_z}{\partial z}=-\frac{1}{\rho}\frac{\partial p}{\partial r}+\frac{1}{3}\frac{\mu}{\rho}\frac{\partial \Theta}{\partial \theta}+\frac{\mu}{\rho}\left[\frac{1}{r}\frac{\partial}{\partial r}\left(r\frac{\partial v_z}{\partial r}\right)+\frac{1}{r^2}\frac{\partial^2 v_z}{\partial \theta^2}+\frac{\partial^2 v_z}{\partial z^2}\right]+f_z \quad \text{Eq.(6)}$$

Using assumptions of Acosta [14] and Lebeck [3]:

- Fluid is Newtonian and of constant density and viscosity $\Theta = 0$
- Gravitational forces may be neglected $f_r, f_\theta, f_z = 0$
- Viscous forces dominate inertia forces
- Flow is laminar
- Velocity and pressure gradients in the *Z* direction are neglected

Using boundary conditions;

- $v_\theta(z=h)=r\omega;$
- $v_\theta(z=0)=0;$
- $v_r(z=h)=0;$
- $v_r(z=0)=0;$

By using the above assumptions and reducing Equations 4, 5, and 6 we obtain equations which can be integrated and applied to the above boundary conditions. The result, in conjunction with conservation of mass, is:

$$\frac{1}{r}\frac{\partial}{\partial\theta}\left[\frac{h^3}{12\mu}\frac{\partial p}{\partial\theta}\right]-\frac{\partial}{\partial r}\left[\frac{rh^3}{12\mu}\frac{\partial p}{\partial r}\right]=\frac{r\omega}{2}\frac{\partial h}{\partial\theta} \qquad \text{Eq.(7)}$$

Equation 7 is the well-known Reynolds Equation.

Equation 7 only contains second derivatives in $p$. This allows a finite difference approach to solve the problem. Such an approach is presented by Lebeck [3]:

$$p_{i,j}\left[\frac{h^3_{i-1/2,j}}{12\mu r_{i,j}}\frac{\Delta r}{\Delta\theta}+\frac{h^3_{i+1/2,j}}{12\mu r_{i,j}}\frac{\Delta r}{\Delta\theta}+\frac{h^3_{i,j-1/2}}{12\mu}\frac{\Delta r}{\Delta\theta}\left(r_{i,j}-\frac{\Delta r}{2}\right)\frac{\Delta\theta}{\Delta r}+\frac{h^3_{i,j+1/2}}{12\mu}\frac{\Delta r}{\Delta\theta}\left(r_{i,j}+\frac{\Delta r}{2}\right)\frac{\Delta\theta}{\Delta r}\right] \qquad \text{Eq.(8)}$$
$$-p_{i-1,j}\frac{h^3_{i-1/2,j}}{12\mu r_{i,j}}\frac{\Delta r}{\Delta\theta}-p_{i+1,j}\frac{h^3_{i+1/2,j}}{12\mu r_{i,j}}\frac{\Delta r}{\Delta\theta}-p_{ij-1}\frac{h^3_{i,j-1/2}}{12\mu}\frac{\Delta r}{\Delta\theta}\left(r_{i,j}-\frac{\Delta r}{2}\right)\frac{\Delta\theta}{\Delta r}-p_{ij+1}\frac{h^3_{i,j+1/2}}{12\mu}\frac{\Delta r}{\Delta\theta}\left(r_{i,j}+\frac{\Delta r}{2}\right)\frac{\Delta\theta}{\Delta r}-\frac{r_{i,j}\omega}{2}\left(h_{i-1/2,j}-h_{i+1/2,j}\right)=0$$

Pressure is the unknown variable. Applied to a grid of size m by n, this reduces to:

$$[A][p] = [B] \qquad \text{Eq.(9)}$$

The equation can be solved using direct methods of matrix inversion. This solution technique is limited in the number of grid points one can use. This author found that a mesh totaling 5000 points is sufficient for a practical solution and is readily inverted using MatLab.

### 2.2b Lubrication Modeling Using Reynolds Equation

With the development of the hydrodynamic model, it is now possible to investigate the effects of wave amplitude and the number of waves on load support, coefficient of friction, and Sommerfeld Number. These parameters are dependant on the solution to Reynolds equation. The introduction of load support, coefficient of friction and Sommerfeld number will be presented herein.

*Load Support*

Solution of the Reynolds Equation provides the distribution of pressure as it is applies to the geometry. The integration of the pressure over the geometry provides the solution for the load support. As mentioned previously, one should remove all values of negative pressure before computing load support.

$$Load\ Support = F = \int prdrd\theta \qquad \text{Eq.(10)}$$

*Coefficient of Friction*

The coefficient of friction calculated here is that due to the viscous shearing of the fluid. There is no consideration of asperity interaction, which may cause a significant contribution to the value of friction. Justification for this relies on the fact that the solution for pressure assumes a minimum film thickness greater than zero, which implies no asperity contact. The calculation for the coefficient of friction is presented in Equation 11.

$$Coefficient\ of\ Friction = f = \frac{1}{F}\frac{1}{r_{mean}}\int_0^{2\pi}\int_{r_i}^{r_o}\left[\frac{\mu r\omega}{h} - \frac{h}{2}\frac{1}{r}\frac{\partial p}{\partial \theta}\right]r^2 drd\theta \text{ , Lebeck [3]} \qquad \text{Eq.(11)}$$

It can clearly be seen from Equation 11 that asperity interaction is neglected. If the film thickness, *h,* goes to zero, the first term in the integration approaches infinity. This represents the dominance of viscous shear due to Couette Flow in regions of small film thickness.

The coefficient of friction calculated is based on the viscous shear components of Couette and Poiseuille Flow which can be seen in the brackets of Equation 11.

*Sommerfeld Number*

Sommerfeld Number represents the ratio of the ability for hydrodynamic pressure generation to the total load. It is of the form of Equation 12.

$$Coefficient\ of\ Friction \approx \frac{Vis\cos ity * Speed}{Load\ Per\ Length} \qquad \text{Eq.(12)}$$

The Sommerfeld Number is similar to Hersey and the Stribeck Number (Seireg [15]). Lebeck defines it as *"Duty Parameter G"* (Lebeck [3]), which is also of the same form. After much deliberation over which parameter to use in order to classify lubrication, it became apparent that the parameters used by other investigators are dependent only on geometries

particular to their experiments or theory. Sommerfeld received credit for this development due to his cleaver substitution in order to integrate a parameter which Reynolds could not (Cameron [16]). Although, as commented by Cameron:

> *"Sommerfeld compared his theoretical friction results with Stribeck's experiments. He missed Reynolds comments on the necessity for the cavitation of the oil under negative pressures. Sommerfeld's lack of engineering background allowed him, surprisingly, to consider that a continuous film could exist, without cavitation, at these pressures. His conclusion's no doubt partly influenced by the fact that under such boundary conditions the hydrodynamic theory gives a minimum coefficient of friction of*
>
> $$\frac{2\sqrt{2}}{3}\frac{c}{R}$$
>
> *Where* *c; is the minimum film thickness in a journal bearing.*
> *R; is the radius of the journal bearing."*

Heresy developed the dimensionless parameter of Equation 12 in 1914 while he was a colleague of Buckingham (famous for the Buckingham Pi theorem). It is now clear why there are so many different representations of the same parameter. Most of the work in lubrication theory was developed during a period when these pioneers all worked in parallel, developing an understanding of lubrication theory.

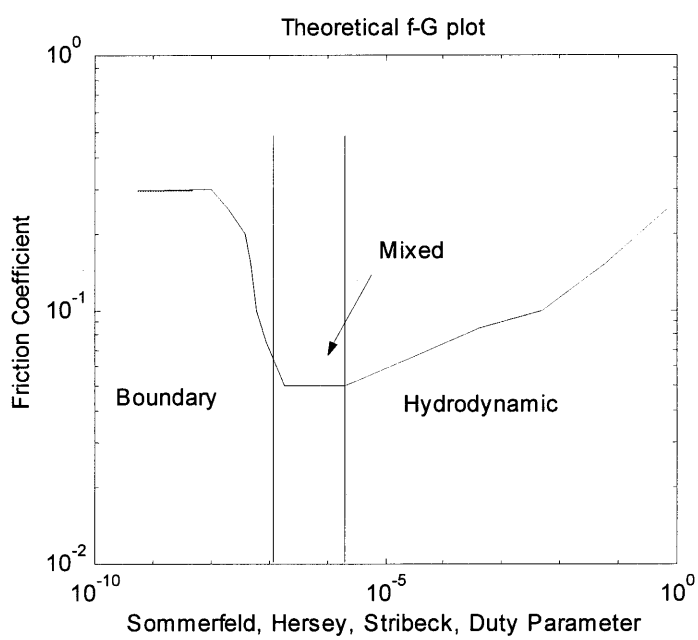


Figure 12. Theoretical Friction Coefficient vs. Sommerfeld Number

Classification begins by calculating the coefficient of friction and Sommerfeld number and plotting them versus each other. Trends in the data should be similar to that of Figure 12. General rules under the various regimes are:

- Boundary; Sommerfeld number increases with decreasing friction.
- Mixed; Sommerfeld number increases with constant low friction.
- Hydrodynamic; Sommerfeld number increases with increasing friction.

The last statement is not particularly true. In boundary lubrication, there may be (and usually is) asperity interaction. This was not considered in the formulation by Reynolds and is not evident in Equation 12.

For face seals the equation for Sommerfeld Number is defined as (Lebeck [3]).

$$\text{Sommerfeld number} = \mu \frac{\omega r_m (r_o - r_i)}{F} \qquad \text{Eq.(13)}$$

$\mu$ (Pa-s); Dynamic viscosity

$\omega$ (Rad/s); Rotational speed

$r_o$ (m); Seal outer radius

$r_i$ (m); Seal inner radius

$r_{im}$ (m); Mean face radius

F (N); Normal loading

## 2.2c Numerical Study of Wavy Surfaces Using Reynolds Equation

Using the hydrodynamic model and the concepts presented, an investigation of the effect of wave amplitude and the number of waves on face seal performance will now be introduced. Theoretical operating parameters have been selected to observe trends in the modeling and are not representative of the mechanical face seals used in the experiments presented in Chapter 4.2.

Theoretical Operating Parameters:

| | | |
|---|---|---|
| Seal Diameter = 100 mm | Seal Face Width = 5 mm | Wave Height = 10 μm |
| Angular Speed = 10 Rad/s | Oil Viscosity = $4.55e^{-3}$[Lebeck] | Number of Waves = 1 |
| Inlet Pressure = 0 Pa | Outlet Pressure = 0 Pa | Minimum Film = 1μm |
| Circumferential Grid Points = 101 | | Radial Grid Points = 26 |

Typical output of a hydrodynamic analysis:

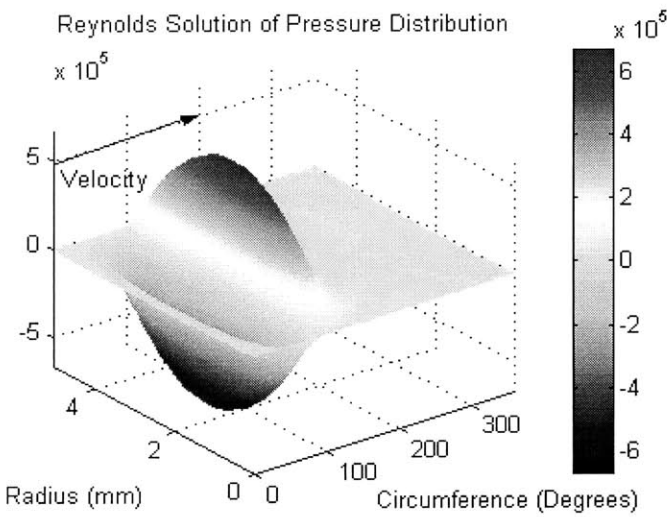


Figure 13. Example Pressure Solution

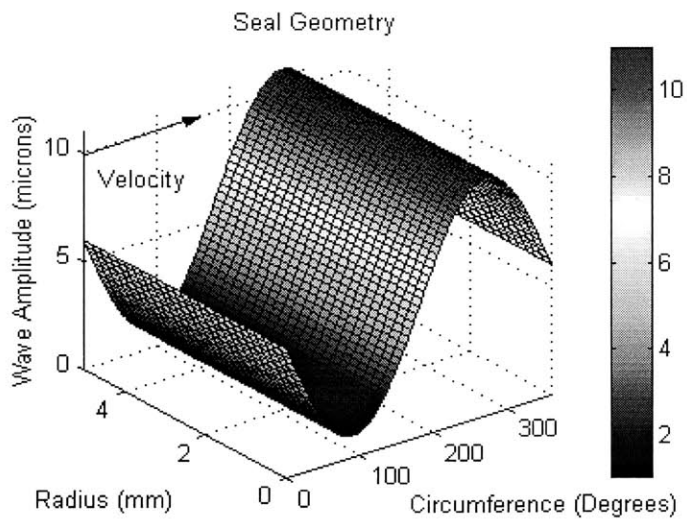


Figure 14. Example Seal Geometry

Load Support =72.7 N

Coefficient of Friction = .0082

Sommerfeld Number =$1.56e^{-7}$

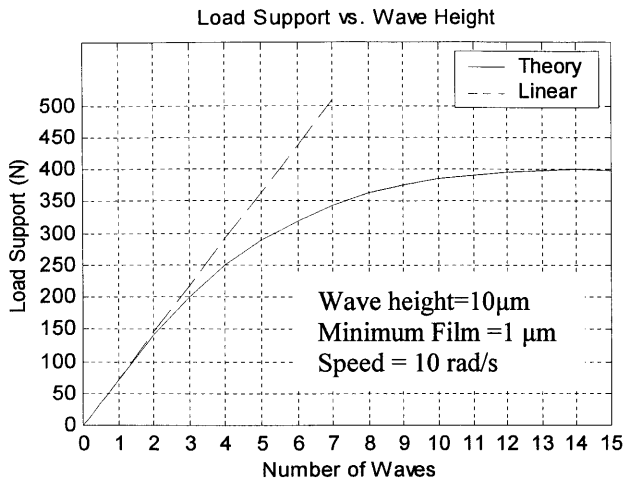


Figure 15. Effect of Number of Waves on Load Support

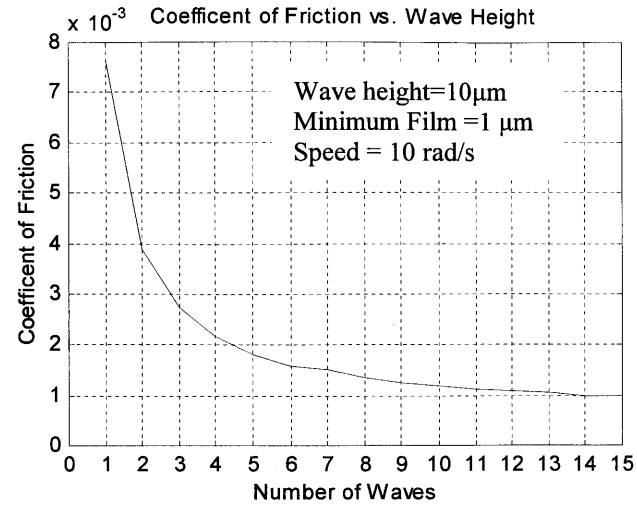


Figure 16. Effect of Number of Waves on the Coefficient of Friction

Figure 15 illustrates the effect of the number of waves on hydrodynamic load support. This relationship appears to be linear for up to three waves. Figure 13 shows that only a small portion of the surface wave contributes to the majority of the load support. Increasing the number of waves simply adds more of these regions to the seal surface thus linearly increases the load carrying capacity. Equation 10 supports this linearity theory for a low number of waves.

$$Load\ Support = F = \int prdrd\theta \qquad \text{Eq.(10)}$$

$$Coefficient\ of\ Friction = f = \frac{1}{F}\frac{1}{r_{mean}}\int_0^{2\pi}\int_{r_i}^{r_o}\left[\frac{\mu r\omega}{h} - \frac{h}{2}\frac{1}{r}\frac{\partial p}{\partial \theta}\right]r^2 drd\theta \text{ , Lebeck [3]} \qquad \text{Eq.(11)}$$

Figure 16 illustrates the effect of the number of waves on the coefficient of friction. Using the linearity of Figure 15 and Equation 11 the trend in friction can be explained. It can be seen from Equation 11 the coefficient of friction is inversely proportional to the hydrodynamic load support capability, *F*.

The benefits of decreased friction and increased load support are clear. Figures 15 and 16 demonstrate the importance of having an increased number of surface waves. It should be noted that to obtain Figures 15 and 16, the number of grid points used for the hydrodynamic program, *Reynolds.m,* had to be significantly increased to 8000 points. All other analysis in this chapter uses a grid spacing of 101 circumferential points by 26 radial points. Figures 15 and 16 used a spacing of 533 circumferential points by 15 radial points. This was used to ensure a solution which is symmetric for each wave. It was found that using too few points in the circumferential direction can result in large errors in hydrodynamic load support values.

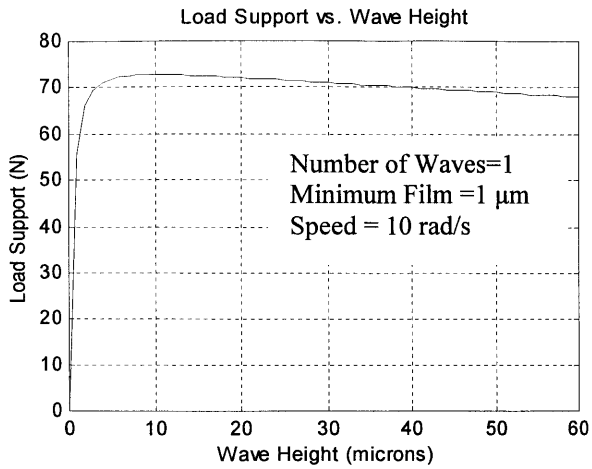


Figure 17. Effect of Wave Height on Load Support

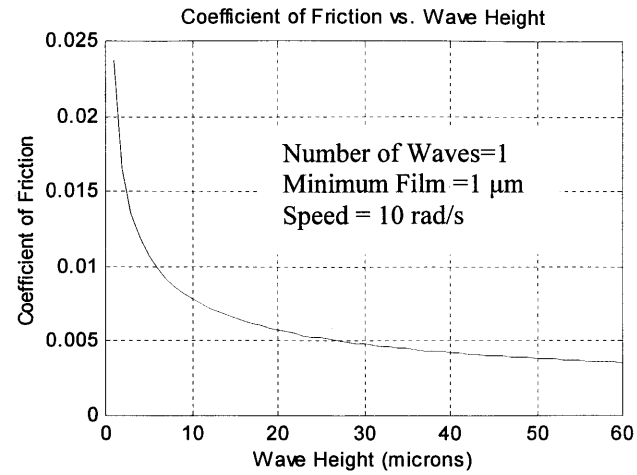


Figure 18. Effect of Wave Height on Friction

Figure 17 illustrates the effect of wave height on hydrodynamic load support capability. It is evident from Figure 17 that a maximum in hydrodynamic load support occurs around 10μm. There is a rapid decrease in hydrodynamic load support for wave heights below of 10μm. This verifies that for a perfectly flat parallel plate separated by a finite fluid film there would be no load support generated (Couette Flow).

$$Coefficient\ of\ Friction = f = \frac{1}{F}\frac{1}{r_{mean}}\int_0^{2\pi}\int_{r_i}^{r_o}\left[\frac{\mu r\omega}{h} - \frac{h}{2}\frac{1}{r}\frac{\partial p}{\partial \theta}\right] r^2 dr d\theta \text{ , Lebeck [3] Eq.(11)}$$

Figure 18 illustrates the effect of wave height on the coefficient of friction. Equation 11 can explain the decrease in friction with increasing wave height. As wave height is increased the Couette contribution to viscous shear diminishes. Viscous shear due to Poiseuille Flow is not very large due to the almost constant load support above 10μm.

Trends show a benefit in maintaining a wave height which optimizes the hydrodynamic load support capability while at the same time greatly reducing the coefficient of friction. This information can be used in conjunction with the Hertzian surface wave deflection model to design a surface wave which maintains a geometry that promotes significant hydrodynamic load support while maintaining low coefficient of friction values.

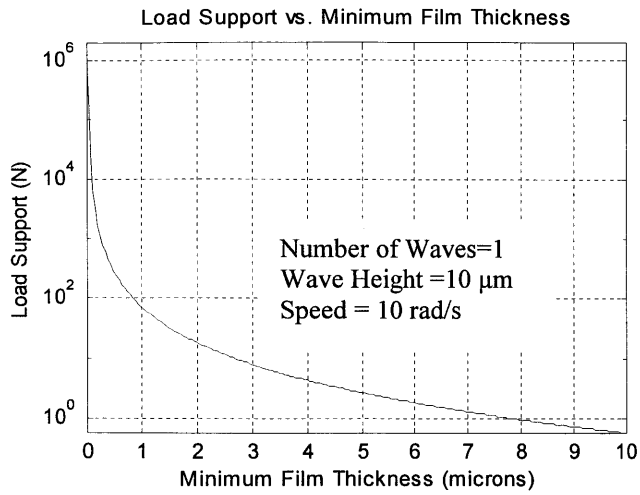


Figure 19. Effect of Minimum Film Thickness on Load Support

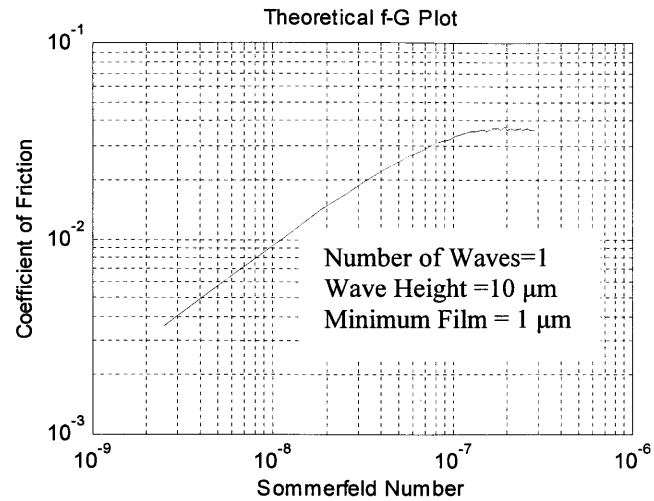


Figure 20. Theoretical Friction Coefficient vs. Sommerfeld Number

Figure 19 illustrates the effect of minimum film thickness on hydrodynamic load support. Minimum film thickness values which approach zero result in load support which approaches infinity. This is characteristic of the mathematics and not realistic. Equations 7 and 9 are responsible for this result. As the minimum film thickness approaches zero, terms in the coefficient matrix, *[A],* approach zero cubically. These values must be inverted to provide the pressure distribution solution. At small values of film thickness this results in hydrodynamic load support approaching infinity, ($[p]=[A]^{-1}[B]$).

$$\frac{1}{r}\frac{\partial}{\partial\theta}\left[\frac{h^3}{12\mu}\frac{\partial p}{\partial\theta}\right]-\frac{\partial}{\partial r}\left[\frac{rh^3}{12\mu}\frac{\partial p}{\partial r}\right]=\frac{r\omega}{2}\frac{\partial h}{\partial\theta} \qquad \text{Eq.(7)}$$

$$[A][p] = [B] \qquad \text{Eq.(9)}$$

Values of minimum film thickness which approach the value of the surface roughness of the face seal should be considered regions of boundary lubrication. Asperity interaction should be considered in order to accurately predict frictional behavior.

Figure 20 is a theoretical representation of a *f-G* (Coefficient of Friction versus Sommerfeld Number) plot. Chapter 2.2 gave a detailed explanation of the trends of this plot and how to determine the operating lubrication regime. By the definition of Chapter 2.2 the operating regime of Figure 20 is hydrodynamic. This result is expected since all modeling used assumptions for a hydrodynamic face seal.

## 2.3 Surface Tension Model of Face Seals

Presented herein will be a model to allow a surface tension check to be performed on an existing or proposed surface wave design. This will represent a worst-case scenario for leakage due to the deformed gap height in the face seal. The programs *SurfaceTension.m* and *PressureGap.m* were used in the analysis and can be found in Appendix A.

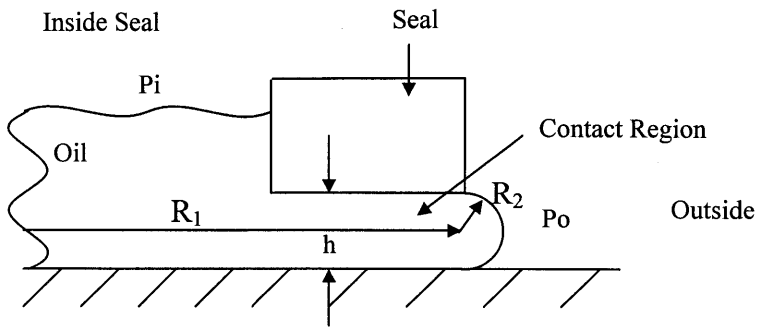


Figure 21. Schematic of Surface Tension Problem

Figure 21 represents the geometry for the problem at hand. This model calculates the minimum film thickness based on an internally pressurized seal. The calculation of film thickness is a consequence of a pressure balance between surface tension and differential pressure acting upon the outer circumference of the seal. The calculated film thickness can be considered a limiting value for the onset of leakage. Increasing film thickness or internal pressure will drive the differential pressure to overcome the surface tension forces and initiate leakage. The model is a well-known solution, which is presented in Equation 14. Results are presented in Figure 22.

Pressure Balance:

$$P_i - P_o = \sigma\left(\frac{1}{R_1} + \frac{1}{R_2}\right)$$

$R_2$=h/2; $R_1$>>$R_2$ ; $R_1$ may be neglected

$$h = \frac{2\sigma}{P_i - P_o} \qquad \text{Eq.(14)}$$

Where

$\sigma$= Surface Tension Coefficient (N/m)

$\sigma$= 0.032 N/m 10W-30 Lubricant

$P_o$ = 101 kPa

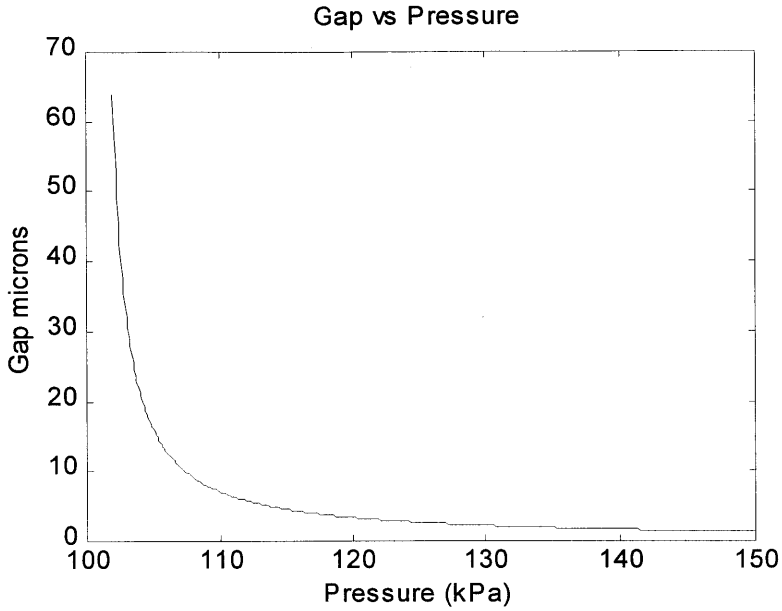


Figure 22. Surface Tension Gap Height vs. Internal Pressure

In order to sustain high internal pressure there must be a small film thickness. In this analysis it is assumed that $P_o$ is atmospheric pressure. If $P_o$ is close in magnitude to $P_i$ then it is possible to sustain much larger gaps in the oil film.

# Chapter 3.

## Experimental Setup

Presented herein is a description of the experimental test apparatus and procedures used for all experimental results presented in Chapter 4.

In order to evaluate and understand key lubrication parameters, it is important that the experiment be properly designed to obtain all information necessary. Figure 23 illustrates the principle design feature of the experimental test rig.

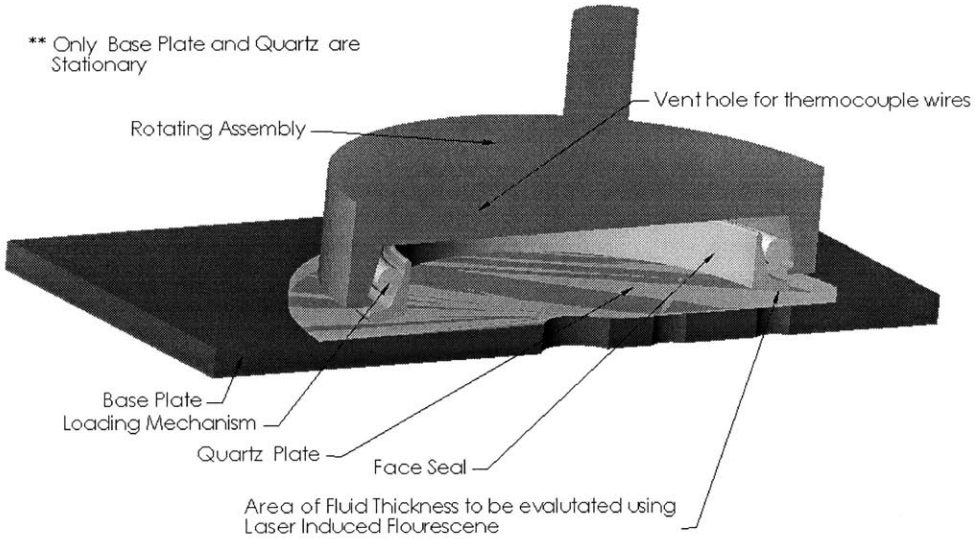


Figure 23. Cross section of Experimental Test Rig

In order to visualize the oil film, it is necessary to use a transparent plate (quartz was used for the experiments presented in Chapter 4). The visualization is accomplished using *Laser Induced Fluorescence*, which will be discussed in detail in Chapter 3.3. In this configuration, the face seal is treated as the primary surface and the quartz is considered the secondary mating surface. Figure 26 shows the actual test rig used for all results presented in Chapter 4.

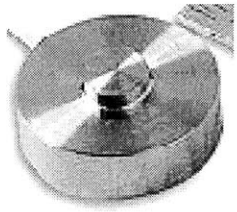

Figure 24. Button Load Cell [25].

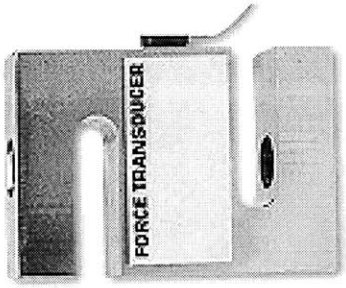


Figure 25. Load Cell used for Torque Measurements [25].

Traditional measurement techniques were implemented to extract information from the face seal experiments. These included normal force, torque, speed and temperature.

Normal force was measured using a subminiature button type load cell, (see Figure 24). The advantage to this particular load cell was its small size. This enabled the sensor to be placed in a pocket machined in the face seal-rotating fixture. Normal load applied to the seal was transmitted through the load cell onto the rotating face seal fixture.

Torque measurements were made using the load cell in Figure 25 mounted to a lever arm that was fixed to the secondary mating surface. This measurement was completed by the use of a bearing to allow the rotation of the secondary mating surface. Without the bearing ,the load cell would have prevent the secondary mating surface from rotating since it is attached to the base of the test rig. The bearing contributes additional static friction into the measurement which is not accounted for. An attempt was made to determine the magnitude of the bearing static friction. This was not possible due to the low resolution of the torque wrench. It can be assumed that the value of the bearing static friction is likely below 5 in-lbf.

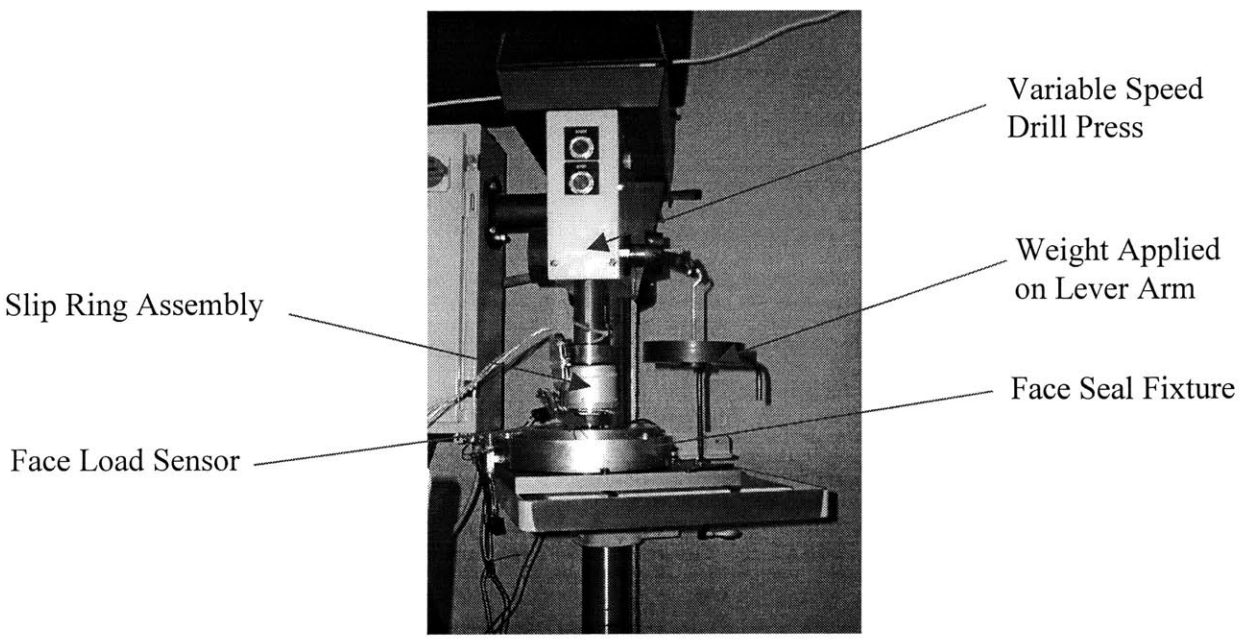


Figure 26. Face Seal Experimental Test Rig

## 3.1 Test Parameters

List of Parameters and their Significance to the Metal Face Seal Problem

| *Parameter* | *Used for Calculating* |
|---|---|
| Normal Face Load | Friction Coefficient, Sommerfeld Number |
| Face Seal Torque | Friction Coefficient |
| Rotational Speed | Sommerfeld Number |
| Seal Temperature | Dynamic Viscosity, Sommerfeld Number |

Table 1.

Seal temperature is measured at a fixed position on the seal while it is rotating. This is made possible by the use of the slip ring assembly shown in Figure 27. Seal temperature is needed in order to calculate the dynamic viscosity of the lubricant.

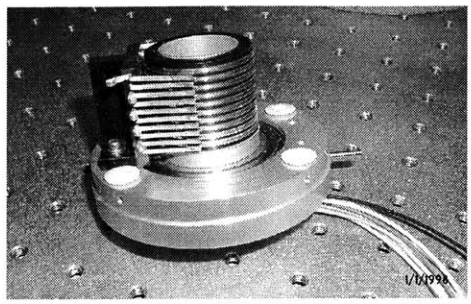

Figure 27. Slip Ring Assembly

Dynamic viscosity can be calculated with the knowledge of the interfacial temperature via the Vogel Equation (Taylor [17]), (Equation 15).

$$\mu = k \exp\left(\frac{\theta_1}{\theta_2 + T}\right) \qquad \text{Eq.(15)}$$

Where:

$\mu$ is the dynamic viscosity with the same units as $\kappa$,
$T$ is the oil temperature in $°C$,
$\kappa$, $\theta_1$, and $\theta_2$ are constants.

For 10W30 oil, these constants are (Taylor [17]):

$$k = 0.1235 \times 10^{-3} \text{ [Pa-s]}$$
$$\theta_1 = 869.72°C$$
$$\theta_2 = 104.4°C$$

Before the experiments five J-type thermocouples are welded to the seal in order to measure a radial temperature profile, as seen in Figure 28. Temperature Probe 3 was used for the calculation of dynamic viscosity. During the experiments performed, this particular thermocouple location typically exhibited the highest temperature reading. This provides an approximate interface temperature, which corresponds to the dynamic viscosity in this region.

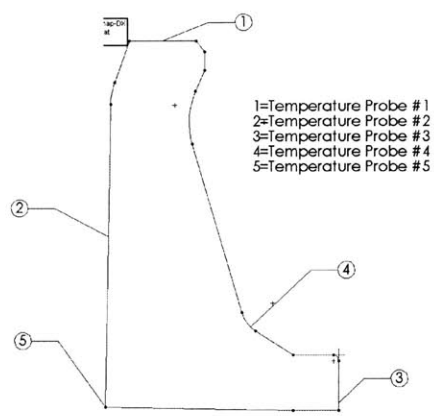


Figure 28. Thermocouple Locations on a Seal Cross section

### 3.2 Visualizing Oil Film Thickness

Visualization of oil film under the sealing interface is not a common practice in tribiological testing. Through the use of *Laser Induced Fluorescence* (LIF) qualitative data representing the oil film thickness can be obtained. Chapter 4 presents experimental results in which this technique was used in order to extract waviness under load as well as leakage of the face seal due to internal pressurization. Examples of typical result are presented in Figures 29 and 30. Figure 30 illustrates how LIF is capable of detecting the meniscus of oil which is located on the outer diameter of the face seal. In addition to this it is possible to qualitatively evaluate the orientation of the contact sealing interface during static or dynamic conditions.

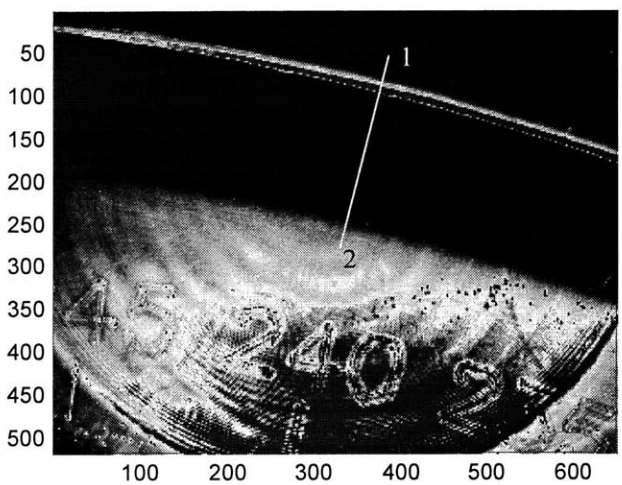


Figure 29. Example LIF Image

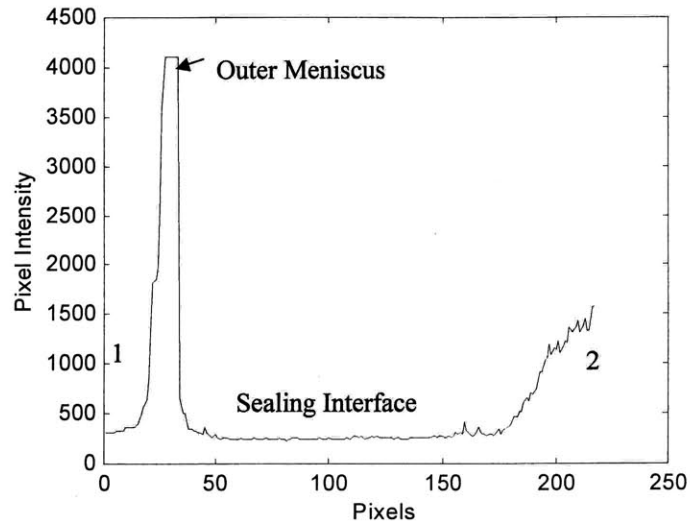


Figure 30. Example Intensity Plot

### 3.3 Principles of Laser Induced Fluorescence (LIF)

The general principle behind LIF is to excite molecules in a dye using a light source. This excitation generates light of a different wavelength than the light source. Proper filtration is required in order to capture the light frequency which contains the film thickness information. Light intensity information is captured using a CCD camera. The result is an image (see Figure 29) where pixel intensity levels correspond to oil film thickness.

#### 3.3a Laser and Optical Measurement Setup

A 532 nm wavelength pulsed Nd-YAG laser is used to excite a dye solution of Pyromethane 567 nm dye, dissolved in 10W30 oil. Care must be taken to use the appropriate concentration and procedure for dissolving the dye into the oil. Appendix B contains the dye

concentration and procedure used for experimental results presented in Chapter 4. Filtering is accomplished using a 570 nm dichroic mirror. This mirror reflects light of wavelength below 570 nm and transmits light above 570 nm. When the laser excites the Pyromethane dye, it produces light above 570 nm in wavelength. Figure 31 illustrates this concept.

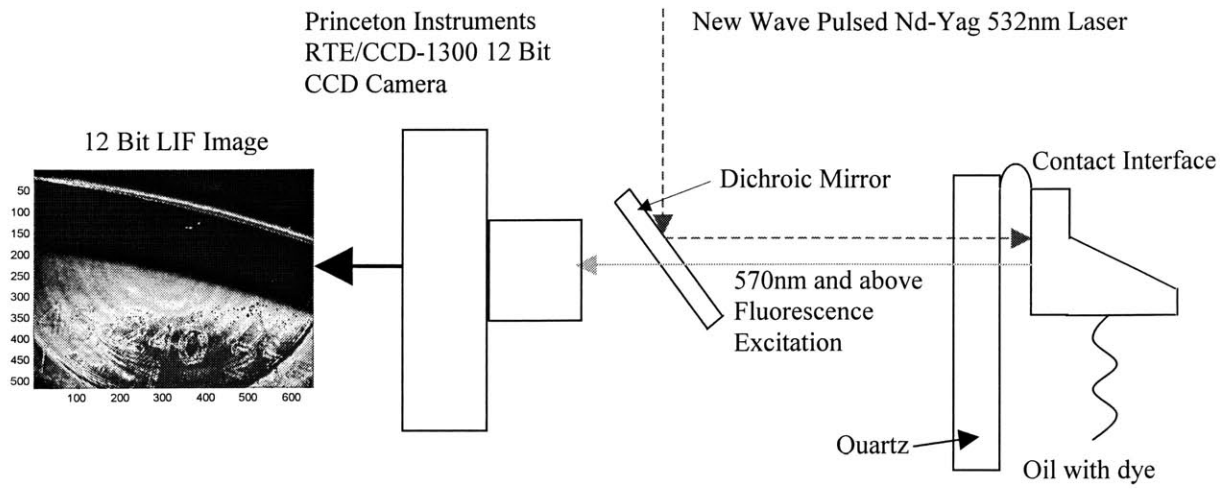


Figure 31. Operational Principle of LIF

The image area is governed by the focal length of the camera and the CCD array size. The actual area of the image in which LIF provides usable data is governed by the beam diameter of the laser. Typically commercial lasers have beam diameters which range from 1 mm to 10 mm. In order to increase data region size, the beam diameter of the laser must be expanded. This is accomplished using beam-expanding optics, as shown in Figure 32. Magnification can be predicted by use of Equation 16.

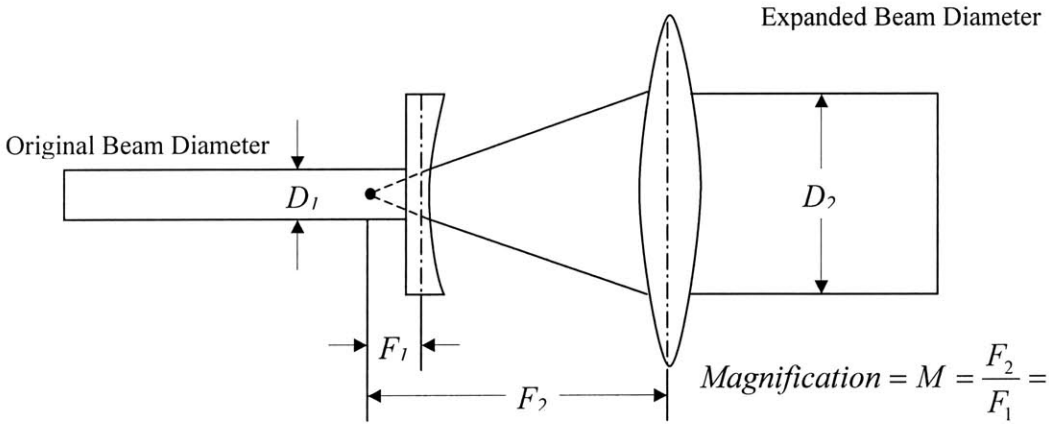


$$Magnification = M = \frac{F_2}{F_1} = \frac{D_2}{D_1} \qquad \text{Eq.(16)}$$

Figure 32. Beam Expanding Optics Principle.

There are several advantages and disadvantages to expanding the beam. An obvious advantage is the increase in area for data extraction. As a consequence of increasing usable area, however the power output per unit area goes down. This can be compensated for in two ways: (1) using a laser with a higher power output or (2) increasing the

concentration levels of the dye. A desirable effect of beam expansion is that the laser beam profile does not resemble a uniform top hat distribution. What is usually obtainable is a Guassian distribution. Expanding the beam creates an increase in the radius of curvature at the center of the beam where power is greatest. This creates an approximate top hat laser profile. It should be noted that the New Wave Pulsed Nd-YAG 532nm Laser does not posses a typical Guassian distribution, (see Figure 33). Therefore expanding the beam is very desirable when using this laser. Fluctuations over space and time are effectively integrated by use of an expanded beam diameter.

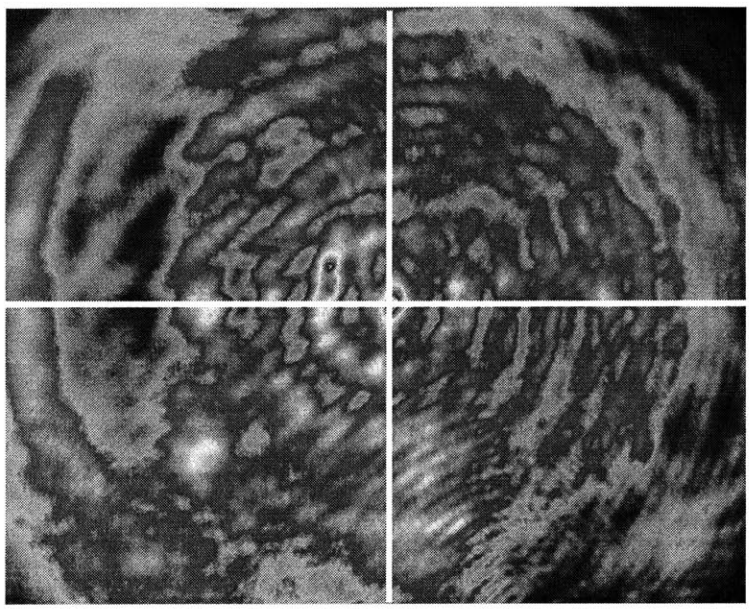

Figure 33. New Wave Pulsed Nd-Yag 532nm Laser Beam Profile

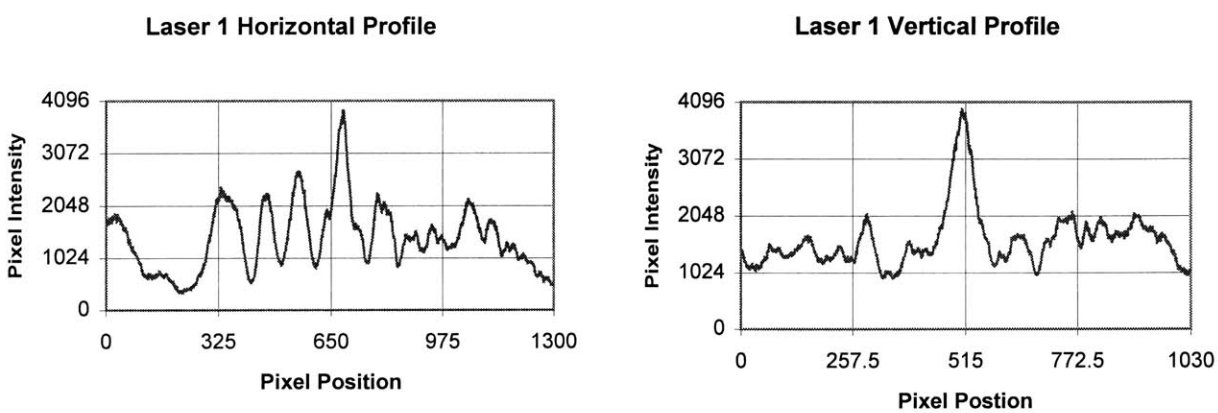


Figure 34. Intensity Plots of Laser Beam Profile from White Lines in Figure 33

Presently, LIF requires calibration if one desires quantitative data. Calibration involves replication of all parameters which could affect the signal intensity (Hidrovo and Hart [18]).

These parameters include:

1. Effects of dye concentration used
2. Reflectivity of the region of interest
3. Temperature response of the dye (Hidrovo and Hart [18])
4. Transmittance effects of the window used
5. Pressurized response of the dye
6. Re-absorption of the dye into itself (Hidrovo and Hart [18])

All LIF results presented in Chapter 4 are qualitative. One can infer certain behavior of the seal under dynamic and static conditions. Visualization of leakage and seal waviness is apparent in the experiments discussed in Chapter 4. Thus, the technique is limited to providing suitable results under specific operating conditions.

## 3.4 Seal Geometry Measurements

Before and after experiments, measurement of critical surface characteristics should be performed. Features to be measured highly depend on the experiment being conducted. In general, one should record free surface wave geometry, surface roughness and cross sectional coordinates. Before and after measurements are vital in understanding the wear mechanisms associated with the operation of the face seal.

### 3.4a Measurement of Free Surface Wave Geometry

In order to understand the effects of surface waves on lubrication it is necessary to know their geometry *a priori*. There are many different instruments, that can be used to perform the measurement. Some of these include surface profilemetry, optical interferometry, or measurements via a Coordinate Measuring Machine (CMM). All seals measured for the experiments in Chapter 4 used a Brown and Sharpe CMM [19], (see Figure 35).

The Brown and Sharpe CMM has an accuracy of 0.1 μm in the measurement region [19], claimed by a Brown and Sharpe application engineer. This particular machine is calibrated across its maximum travel region, which is a diagonal of a rectangular box. The manufacturer specification for the LEITZ Cygnus 20.12.10 is 1μm across 1.5m x 2m x 3m. Therefore, by reducing the measurement range to 192mm x 192mm x 50 mm, the accuracy of the machine is improved.

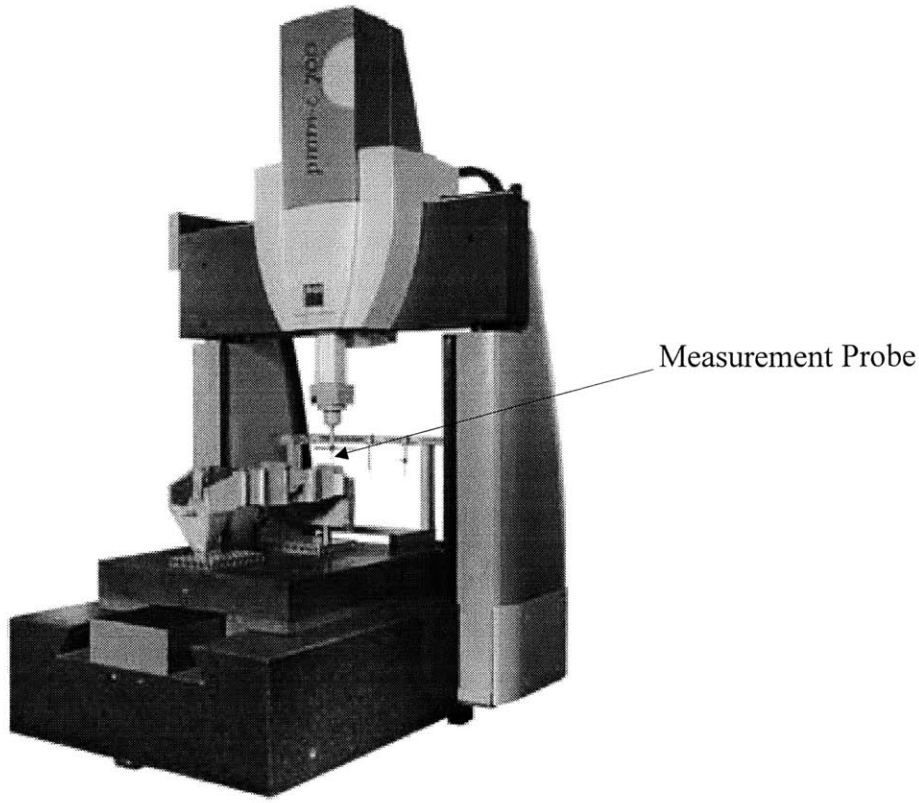


Figure 35. Example of a Typical High Accuracy Brown and Sharpe CMM

There are two distinct modes of operation for this particular measuring device. The first is known as scan mode. The second is known as point probe. The measurement probe is a small ruby sphere that is connected to a 3-axis force transducer. If very high accuracy is desired, then the use of the point probe is preferred. Error is inherent in each axis of the probe device. The scan mode literally scans the surface with the probe. In order to extract 3-D position it must use readings from all three force transducers. Point probe mode uses only one force transducer and moves in the direction of the axis of the measurement, thus reducing error induced by the other two force transducers. The disadvantage in using the point probe method is the longer time required to complete a measurement.

# Chapter 4
# Experimental Results

Presented herein is a description of experiments conducted and results related to the evaluation of surface waves present on face seals. Three experiments are presented to accompany the theory disscussed in Chapter 2. The first is an LIF wave deflection experiment which relates normal load to the deflection of the surface waves present in the seal. The second is tribiological testing of the face seal in order to distinguish the effect of surface wave amplitude on load support. The last experiment is an LIF experiment involving the internal pressurization of the face seal and observation of the resulting gap height.

## 4.1 LIF Wave Deflection vs. Load

This experiment was designed to extract the wave deflection of a face seal under static conditions while load is applied. Through the use of LIF it can be seen that this technique is very effective in extracting the surface wave deflections present. The files *LIFLoad.m* and *LIFLoadDefl.m* were used to perform the following extraction of LIF data to seal waviness. In addition, the files *Hertz.m* and *HertzTheory.m* were used for the theoretical comparison presented herein.

Figure 37 illustrates the measured surface wave prior to the experiment. Here two periodic waves can bee seen with a wavelength equal to half of the circumferential length.

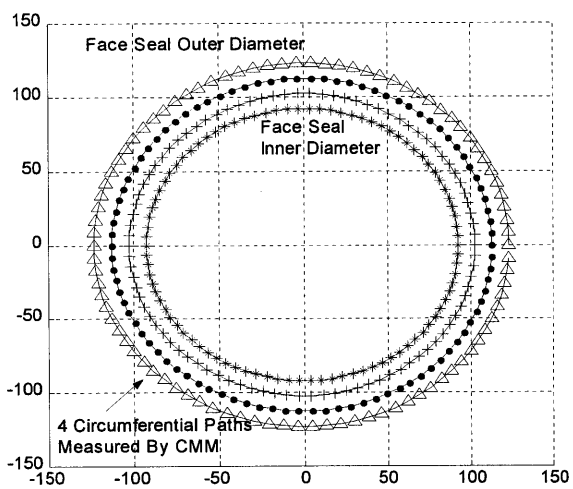


Figure 36. Waviness Symbol Plot

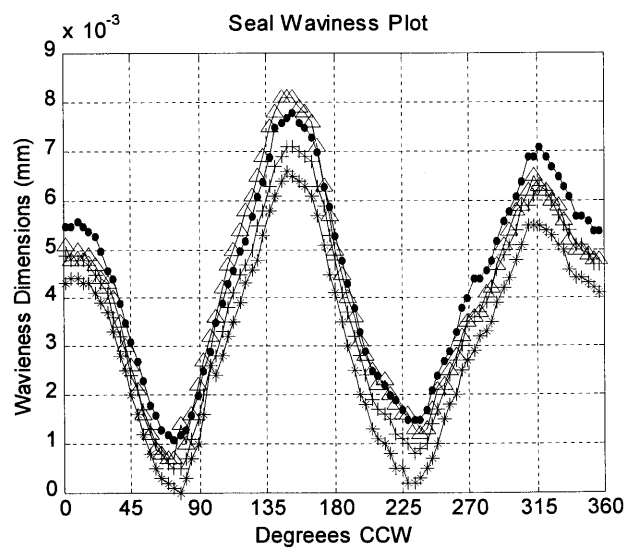


Figure 37. Seal Waviness Plot

The value of the free surface wave height is 8μm. This measurement was taken using the point probe method of Chapter 3.4a at every four degrees around the seal face.

In order to reference the position of the seal, a novel modification to the face was necessary. This modification involved having a numeric pattern etched into the seal face to reference the angular position of the seal, see Figure 38. Since the LIF technique is sensitive to film thickness the regions of the etching are enhanced illuminating the numbers, as seen in Figure 39.

Figure 38. Etched Numeric Pattern

The experiment consisted of capturing eighteen LIF images at every twenty degrees around the seal at a given axial load. The average intensity value was computed for each position. These results are plotted versus angular positions. Several loadings were used in this procedure to evaluate the surface wave of the seal and the deflection due to increased loading. Result are shown in Figure 40.

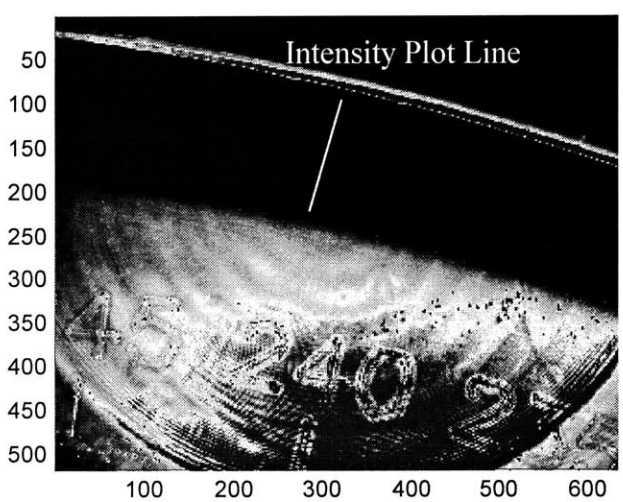


Figure 39. Typical LIF Image Captured

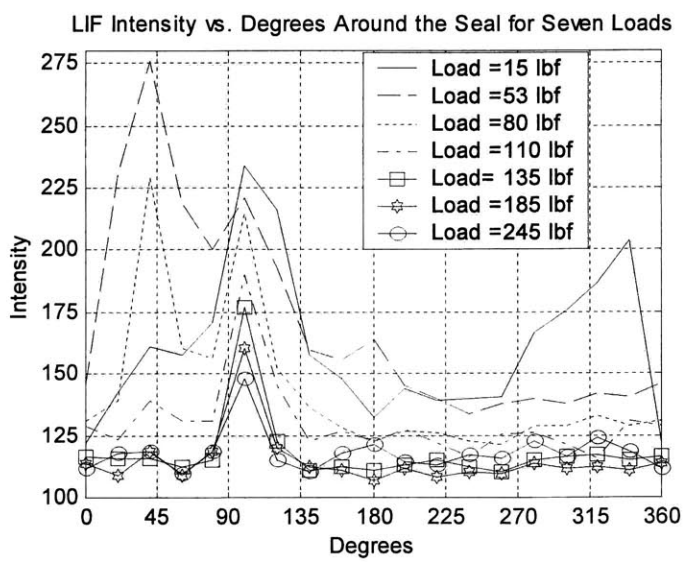


Figure 40. LIF Experimental Load Results

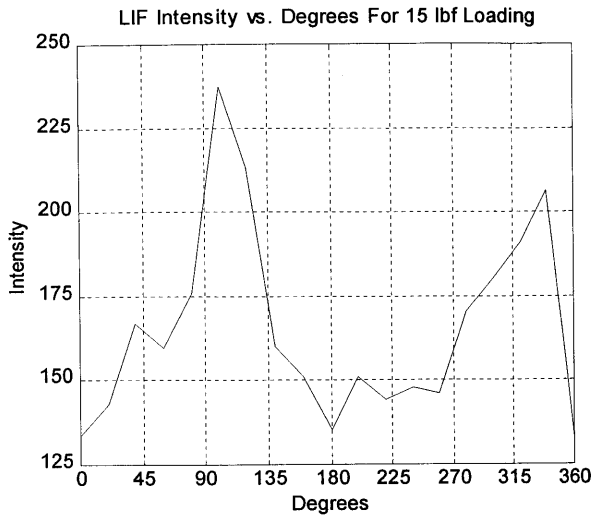


Figure 41. Experimental Result at 15 lbf Loading

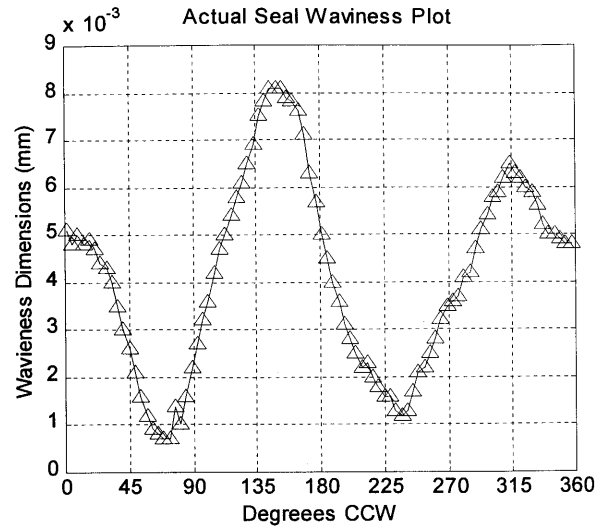


Figure 42. Actual Unloaded Surface Geometry

It can be seen that Figure 41 is nearly inversely proportional to Figure 42, with a slight discrepancy in the data likely due to a shift in the measurement. This illustrates that the LIF result strongly correlates to the surface measurement taken by the CMM. From the theory presented in Chapter 2.1a, 15 lbf (67 N) loading does not significantly deflect the surface waves present in the seal. Therefore for further analysis, Figure 41 will be treated as the original un-deflected surface wave.

By normalizing the first LIF load condition to 100 percent wave height, we may calculate the normalized wave height for the higher loads. This result is plotted in Figure 43, along with the standard deviation of the intensity signal.

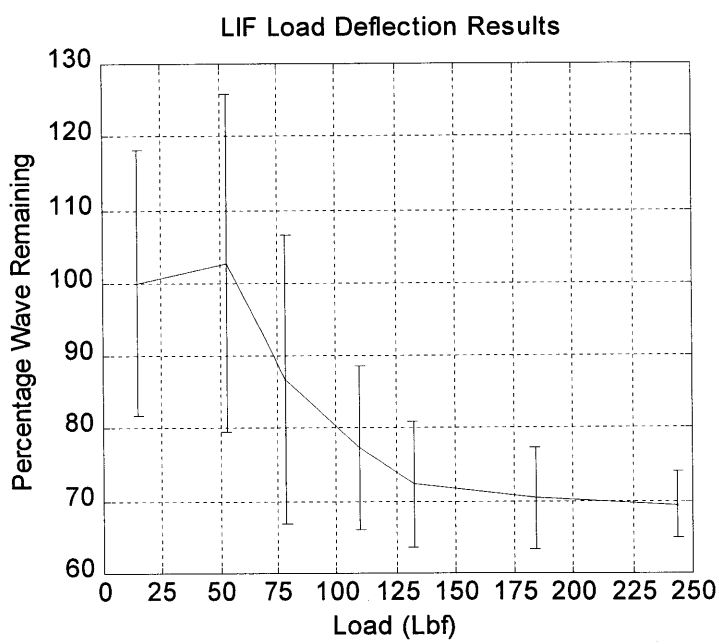


Figure 43. LIF Load Deflection Results

The Hertz contact mechanics model developed in Chapter 2 may now be applied so as to obtain a correlation to the experimental results. Parameters used for the analysis are:

Actual Test Seal Parameters:

| | | |
|---|---|---|
| Seal Diameter = 192 mm | Seal Face Width = 2 mm | Wave Height = 8 μm |
| Number of Waves = 2 | Primary Material Modulus = 210 Gpa | Primary Poisson Ratio = 0.33 |
| | Secondary Material Modulus = 72 Gpa | Secondary Poisson Ratio= 0.17 |

A 2mm face width was used in the analysis. This width corresponds to the measurement path taken by the CMM machine. The four radial measurement lines (shown in Figure 36) are spaced at 0.5mm.

The result of the analysis can be seen in Figure 44.

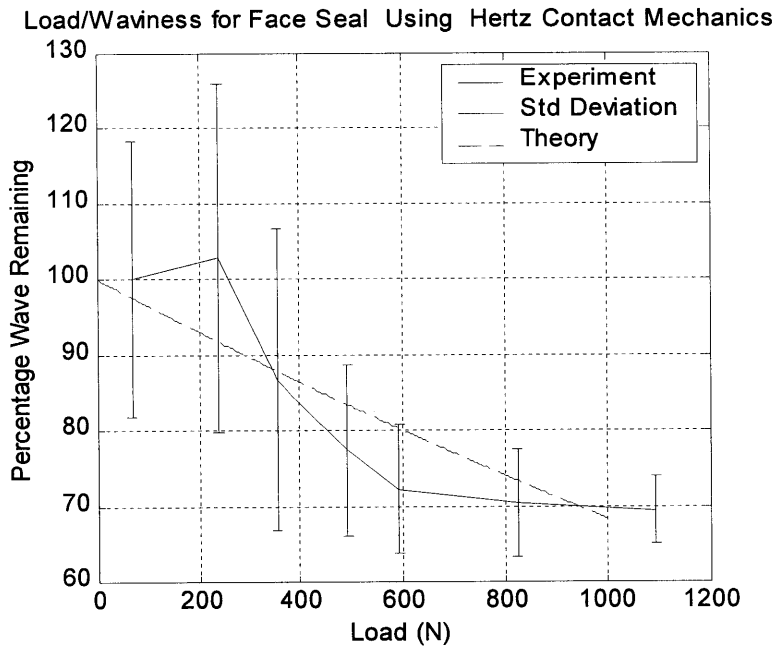


Figure 44. Experimental and Theoretical Results of Wave Deflection

From Figures 37, 40, and 44, we can infer behavior which may have occurred during the experiment. In Figure 37 it is apparent that there are only two wave crests. This will result initially in only two contact points, as observed in the 15 lbf (67 N) loading graph of Figure 40. This is not a stable loading configuration, as kinematic stability requires that the seal eventually come into contact in a third region. In the next loading (53 lbf (237 N)) seen in Figure 44, the values of pixel intensity drop on one half of the graph and raise on the other. It appears that the seal has collapsed to one side finding that third contact point. The remaining loading diagrams show a consistent surface wave deformation . As a result of this, the 53 lbf (237 N) loading produced pixel intensity values much higher than the 15 lbf (67 N) loading. This caused the calculated average to be higher than the original "100%" value in Figure 44.

## 4.2 Wave Amplitude Experiment

This experiment presented in this section was designed to distinguish the effects of wave amplitude on face seal performance. Two seals were chosen which were geometrically equivalent, except for their values of wave amplitude. The first seal, labeled "Test Seal A" has a wave height of 20μm. The second seal, labeled "Test Seal B" has a wave height of 8μm. These are shown graphically in Figures 45 and 46. The seals were run through a series of different test conditions, in order to extract a f-G plot (Friction vs. Sommerfeld), which will aid in the evaluation of the seals. In addition, a theoretical comparison is provided in order to correlate the theory to the experiments. The following programs (see Appendix A) were used in order to facilitate the analysis:

*Hertz.m*

*Hertztheory.m*

*Reynolds.m*

*Hydrodynamic.m*

*FaceSeal_fig.m*

Geometry of the Seals:

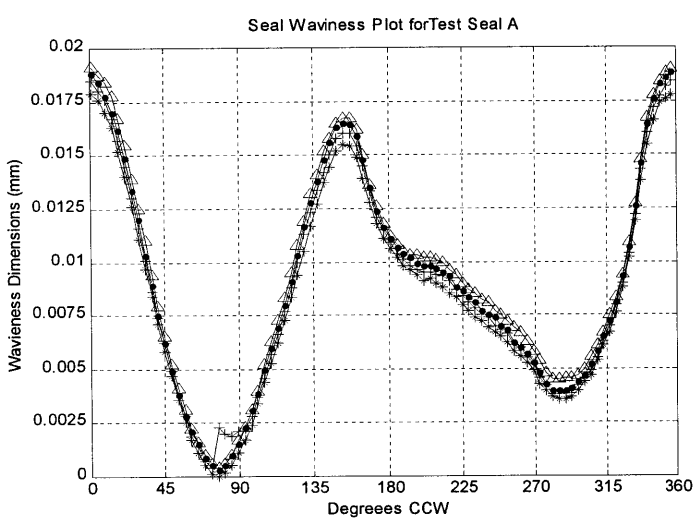


Figure 45. Test Seal A Wave Geometry (20 μm)

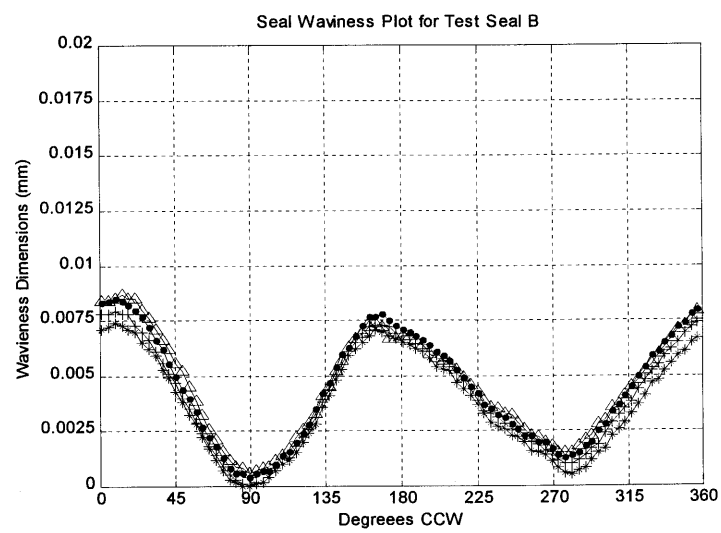


Figure 46. Test Seal B Wave Geometry(8 μm)

Differences in actual wave geometry are minimal as compared to the two distinct wave amplitudes.

The operating conditions for these experiments are presented below:

| Test | Seal | Diameter | Normal Face Load | Surface Speed Range | Lubricant |
|---|---|---|---|---|---|
| 1st | A | 192mm | ≅ 600 N | 0.1 to 4m/s | Pennzoil 10W30 w/Z-8 |
| 1st | B | 192mm | ≅ 600 N | 0.1 to 4m/s | Pennzoil 10W30 w/Z-8 |
| 2nd | A | 192mm | ≅ 120 N | 0.1 to 4m/s | Pennzoil 10W30 w/Z-8 |
| 2nd | B | 192mm | ≅ 120 N | 0.1 to 4m/s | Pennzoil 10W30 w/Z-8 |

The duration of each experiment was approximately 6.7 hrs, with speed increments of 0.1 m/s every 10 minutes. This time frame was selected due to previous experience with the particular face seal used. In preliminary experiments conducted early in this research, it was found that the temperature response stabilized in about 10-minutes across these given load and speed ranges. Virtually all other parameters remain constant during this period.

*Wave Amplitude Experiment at High Load*

The results of the high load experiments are shown in Figures 47 and 48 as experimental coefficient of friction versus Sommerfeld number at 600 N Loading.

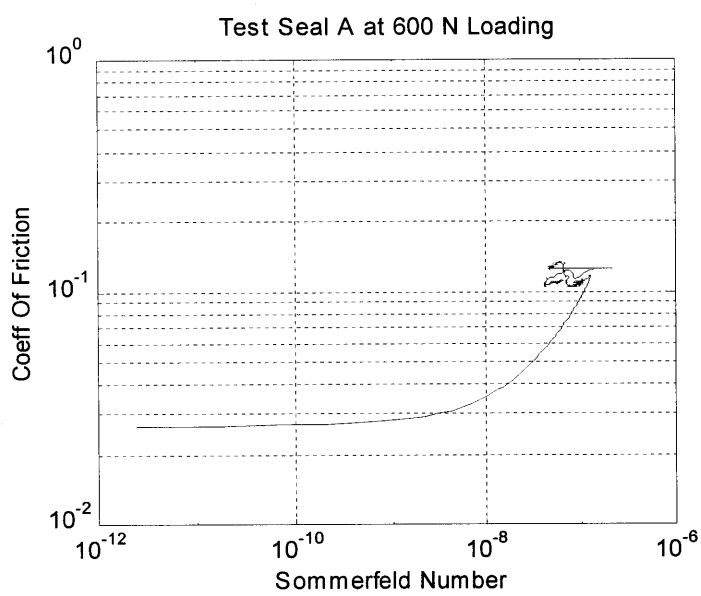


Figure 47. f-G Plot for Test Seal A (20μm) at 600 N

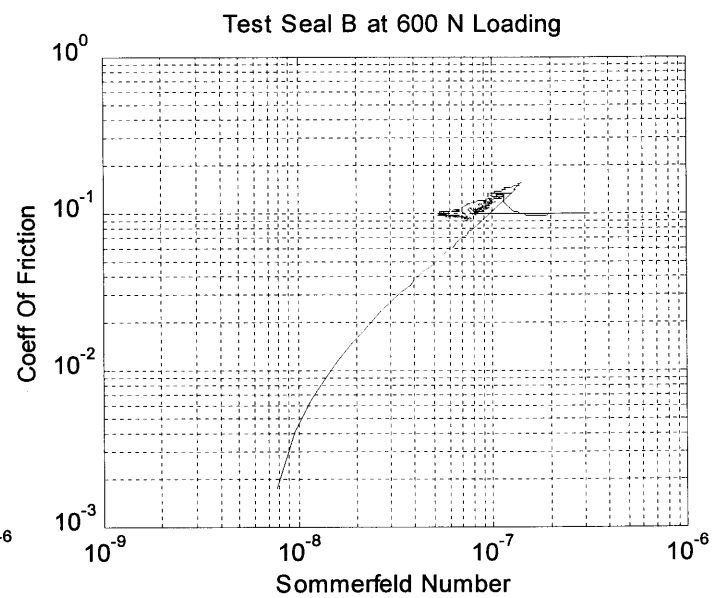


Figure 48. f-G Plot for Test Seal B (8μm) at 600 N

From definitions of Chapter 2.2b, Test Seal A (shown in Figure 47) would be classified as exhibiting mixed to hydrodynamic lubrication. Test Seal B (shown in Figure 48) would be classified as hydrodynamic lubrication. Test Seal B appears to be providing enough load support to remain hydrodynamic.

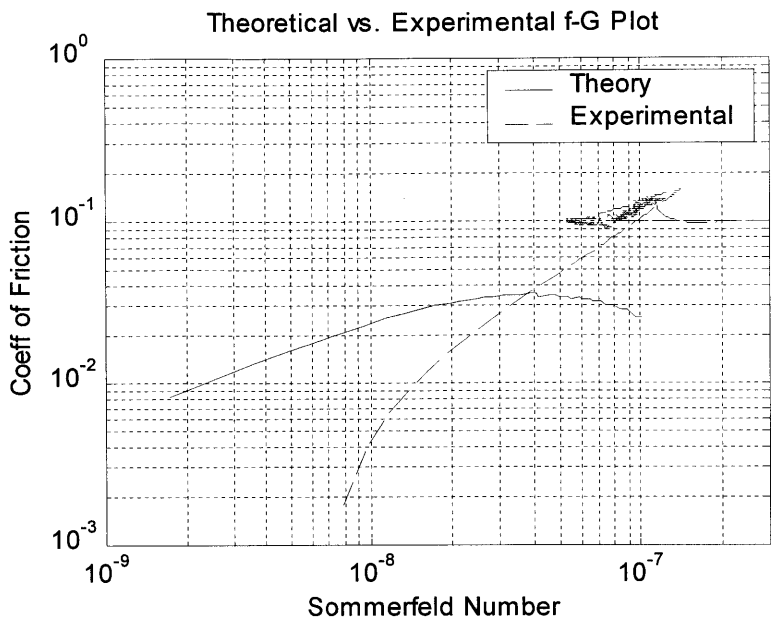


Figure 49. Experimental vs. Theoretical f-G Plot for Seal B at 600 N

A theoretical comparison using the model of Chapter 2.2a and 2.1 can only be made if operation is hydrodynamic. This is the case for Test Seal B. Figure 49 illustrates the comparison. It can be seen that the model does not correlate well with the experiment. Several possible explanations follow.

Many assumptions were made in order to use the simplified form of *Navier Stokes* Equations. One of the most important assumptions is the necessity for a minimum film thickness greater than zero. This implies that there is no contact between the two surfaces, thus classified as hydrodynamic. In the experiment this may not be the case.

In order to generate the coefficient of friction versus Sommerfeld number plot of Figure 49 another assumption had to be made. The assumption was that the seal generates enough hydrodynamic load support to fully support the applied load to the seal of 600 N across all speed ranges theoretically investigated. Hydrodynamic load support is generated by adjusting the minimum film thickness to a value that which produces a pressure solution equal to the applied load. At this point the solution is achieved and the Sommerfeld number and coefficient of friction are calculated. In order to generate the *f-G* plot, speed and viscosity are varied in accordance to experimental observation. The discrepancy in the experimental and theoretical results may be related to the assumption of full hydrodynamic lubrication. At very low surface speeds the theory is calculating a film thickness which produces a load support equivalent to the applied load. From Section 2.2c, Figure 19 it can be seen that load support approaches infinity as minimum film thickness goes to zero. When the minimum

film thickness approaches zero the Couette contribution to viscous shear also approaches infinity, which would result in no relative motion between the seal contact surfaces.

From definitions of Chapter 2.2b Figure 50 and 51 would be classified as hydrodynamic lubrication. Another experiment similar to that presented previously except for a sufficiently reduced normal load, was conducted and compared to theory. It can be seen from Figure 50 that the mode of lubrication is characteristic of hydrodynamic lubrication, and quite different from the high load case of Figure 47. Test Seal B at the lower load has remained hydrodynamic. This experimental result leads to the conclusion that the lower wave amplitude promotes a more consistent lubrication mode. This consistent performance for Test Seal B however, comes with a penalty in that the friction in both load cases is higher than for Test Seal A.

*Wave Amplitude Experiment at Low Load*

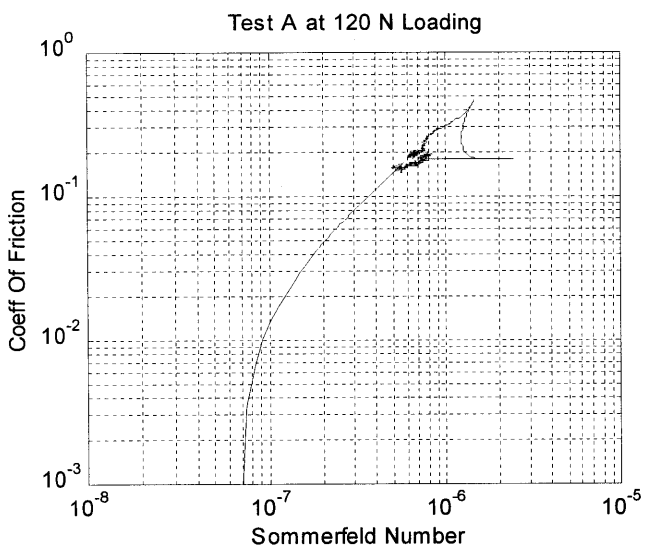


Figure 50. f-G Plot for Test Seal A at 120 N

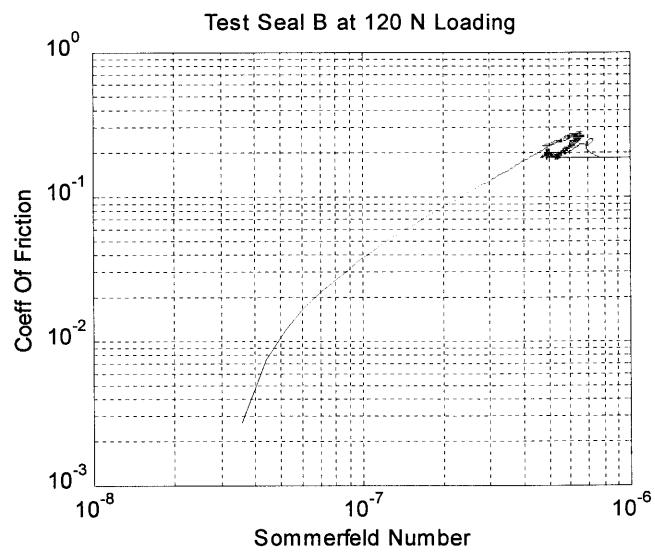


Figure 51. f-G Plot for Test Seal B at 120 N

Since the experimental results of Figures 50 and 51 revealed that the mode of operation is hydrodynamic for Test Seals A and B a theoretical comparison using the model of Chapters 2.2a and 2.1 can be applied. Figure 52 illustrates the comparison for Test Seal A. The model does not correlate well with the experiment. Figure 53 illustrates the comparison for Test Seal B. Again the model does not correlate well with the experiment. The explanation the lack of correlation of these experiments to theoretical results are the same as those made for the wave amplitude experiments at high load.

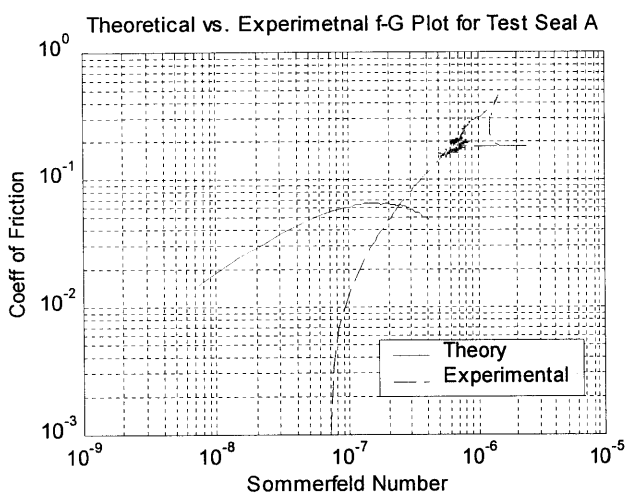


Figure 52. Experimental vs. Theoretical f-G Plot for Test Seal A at 120 N

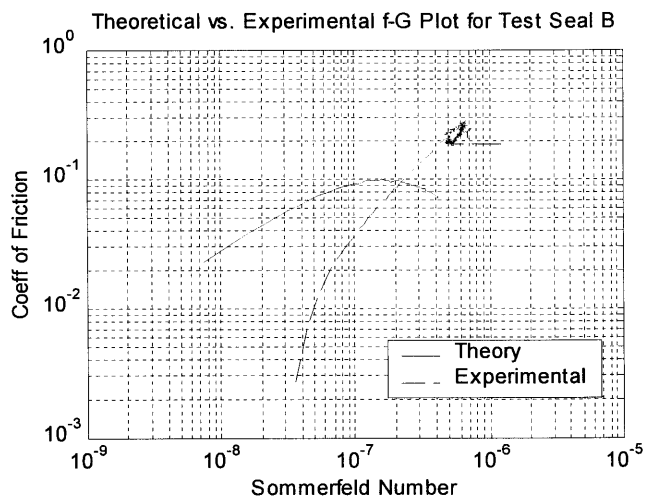


Figure 53. Experimental vs. Theoretical f-G Plot for Test Seal B at 120 N

Figure 54 demonstrates how the f-G curve is affected by an increase in constant load. Experimental data from Test Seal A at 120 N is also plotted to show that it is possible that the amount of hydrodynamic lift produced is not 120 N, as was first anticipated, but may be much lower, below 50 N. The slope of the curve may be affected due to the assumption of constant load support. If the ratio of hydrodynamic lift to asperity support changes due to increasing speed, the experimental data becomes a composite representation of the theoretical curves of Figure 54.

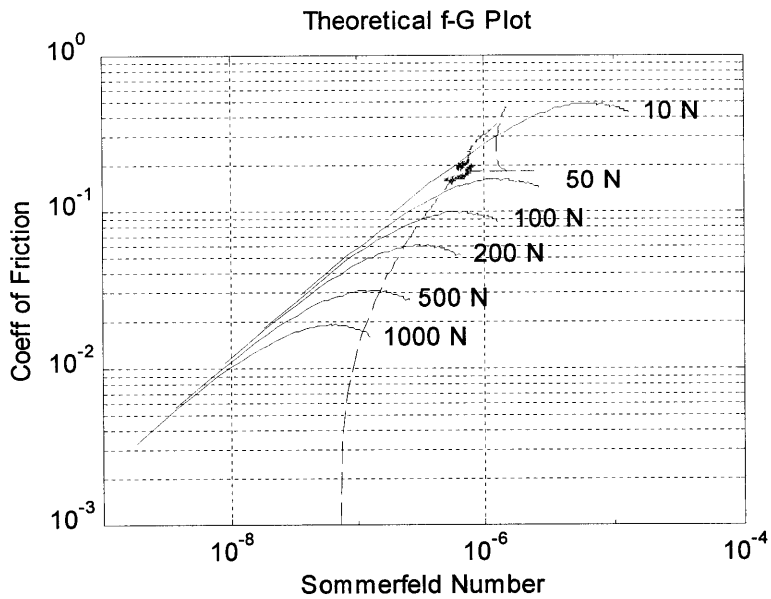


Figure 54. Effect of Load to f-G Plot and Experimental Fit

The goal of this particular experiment was not fully achieved but many issues were revealed concerning measurements and operating modes. An experiment which isolates the controllable variables is needed in order to further verify the theories presented. A detailed recommendation for future research will be presented in the Chapter 5.

### 4.3 Internally Pressurized Leakage Experiment

The internally pressurized leakage experiment was designed to evaluate leakage based on internal pressurization of the seal assembly. An air valve was fitted onto the seal retention fixture and a standard bicycle air pump was used to provide pressure to the inside of the seal. Pressure was applied until leakage was noticeable or until the upward force generated reached the maximum rating of the load transducer 250 lbf (1120 N). This experiment was performed on a 192 mm laser engraved seal, which provided reference points for surface wave locations. Leakage was observed via *Laser Induced Fluorescence* and qualitatively estimated based on image number and frame rate. The experiment was performed at two distinct locations of the seal. The first was the region of minimum film thickness, (under a crest of a wave). The second was at the valley of a surface wave, corresponding to the thickest film. The seal used here was the same seal discussed in Chapter 4.1. Figure 55 depicts the surface wave geometry.

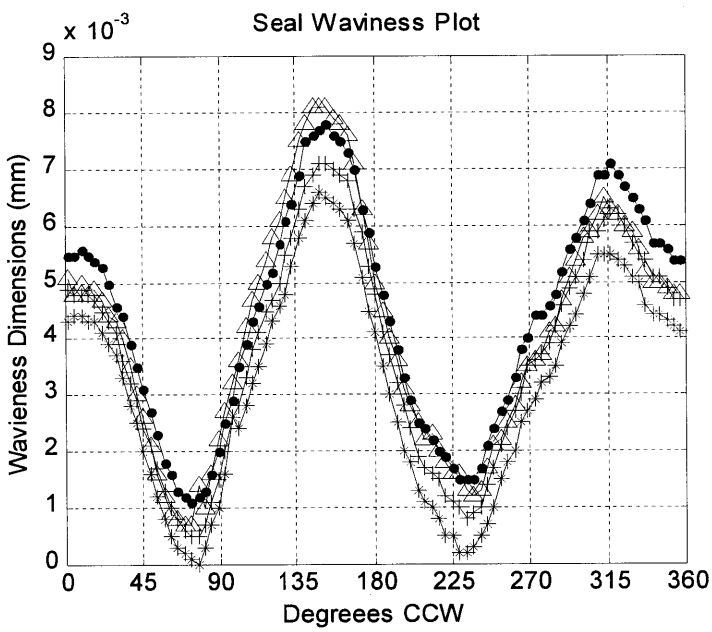


Figure 55. Leakage Test Surface Wave Geometry

The location of the minimum film thickness corresponds to 155-degree location of Figure 55. LIF images of Figures 57 through 60 show the markings at the 35-degree location. These are actually the same location on the seal (the laser engraving and CMM measurements are off by 120 degrees). This offset is also present for the thickest film region where the 80-degree location of Figure 55 corresponds to the 320-degree mark for Figures 62 through 65.

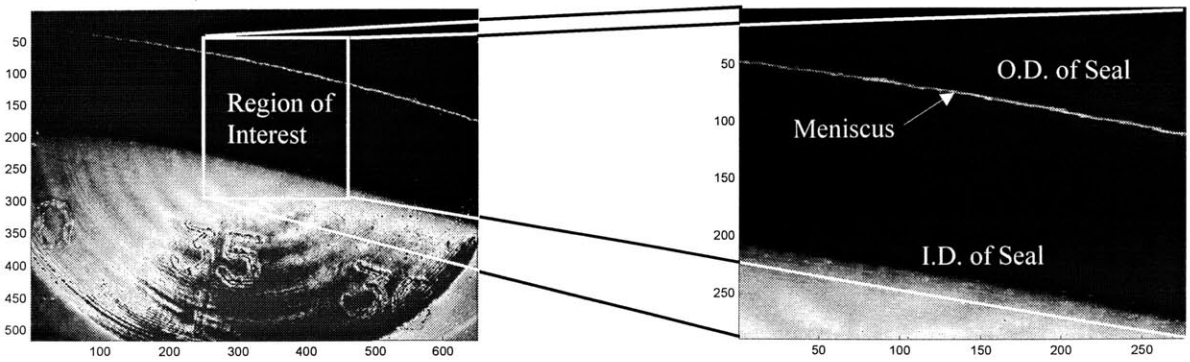


Figure 56. Description Of LIF Leakage Images

*35 Degree Region- Region of Minimum Film Thickness*

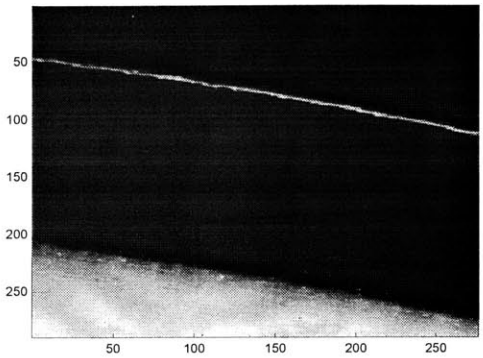

Figure 57. Pressure Test at 5 kPa, 0s

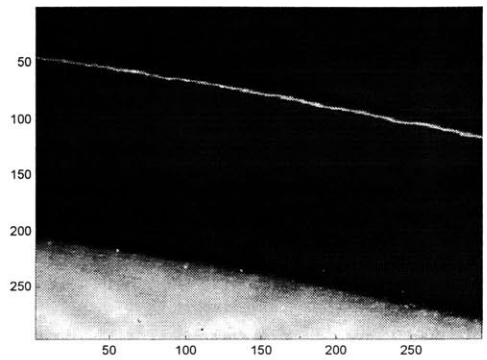

Figure 58. Pressure Test at 40 kPa, 40s

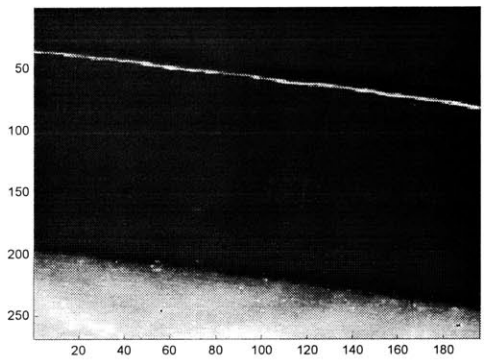

Figure 59. Pressure Test at 60 kPa, 62s

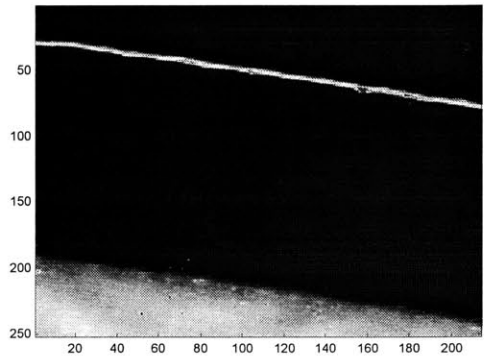

Figure 60. Pressure Test at 5 kPa, 90s

Throughout the duration of the test there was no appreciable leakage detected in the region of minimum film thickness via LIF. Maximum internal pressure attained was 60 kPa, correlating to an upward force of 1500 N (the force transducer's maximum rating was the limiting factor for this experiment). Figure 61 illustrates the increasing internal pressure with respect to time.

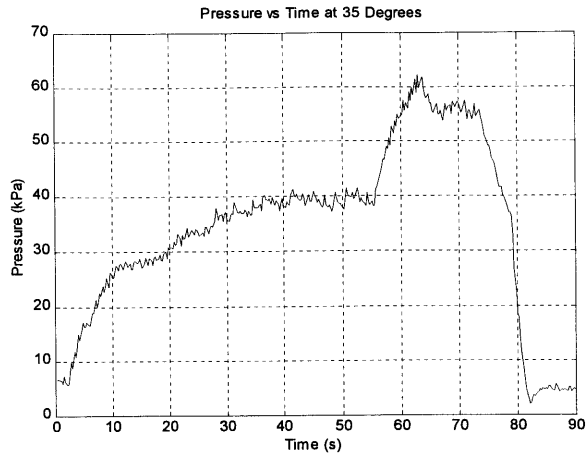


Figure 61. Pressure vs Time Relationship at 35 Degrees Location

In Figure 61 there is a region where the pressure appears to suddenly drop. The pressure drop corresponds to leakage at the 320-degree location of the seal (the valley of the surface wave shown in, Figure 55). Internal pressure decayed due to outward flow of lubricant through the sealing interface. The pressure, was not large enough to initiate leakage at the 35-degree location. By using the surface tension model of Chapter 2.3 it is clear that the film thickness at this region is 1 μm or less. Only if the pressure were increased instantaneously to a very large value would it be is possible for leakage to occur at the 35-degree region.

*320 Degree Region- Region of Maximum Film Thickness*

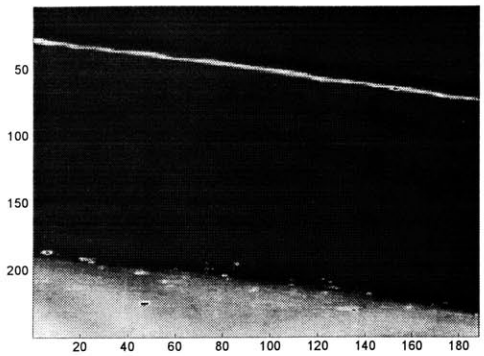


Figure 62. Pressure Test at 5 kPa, 0 s

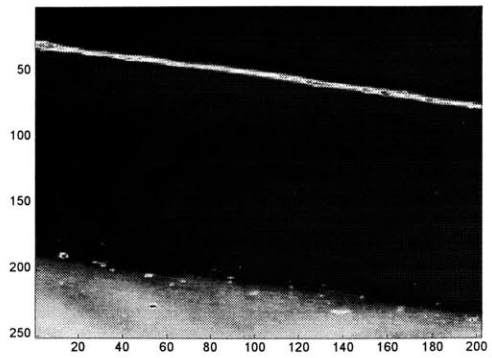


Figure 63. Pressure Test at 30 kPa, 17 s

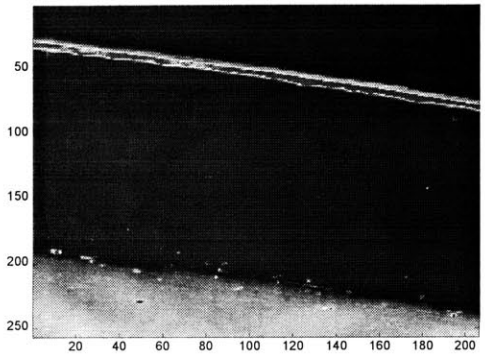


Figure 64. Pressure Test at 40 kPa, 34 s

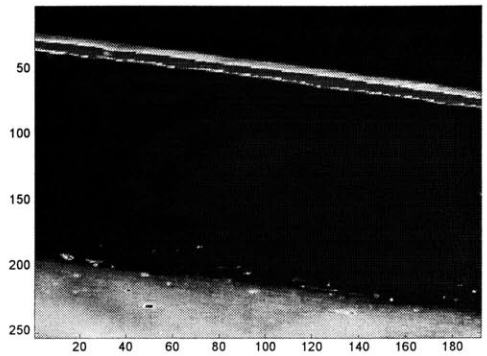


Figure 65. Pressure Test at 37 kPa, 51 s

By observing the seal in the 320-degree location the progression of leakage in Figures 62 to 65 is demonstrated by the increasing intensity and size of the oil ring on the outer edge of the seal. Here the internal pressurization of the seal ceased at the sensor's maximum rating as denoted by the decay of the pressure response in Figure 66. At this point leakage has appeared to stop. Leakage is visually estimated to initiate between Figures 62 and 64 where the pressure is between 5-40 kPa. The actual point of surface tension rupture is very difficult to observe without high-speed image recording equipment. Using the surface tension model of Chapter 2.3, the sustainable film thickness for this pressure range was calculated and found to be between 2.5 and 15 μm. For the natural unloaded seal waviness of 8 μm, this correlates well with the experimental observations

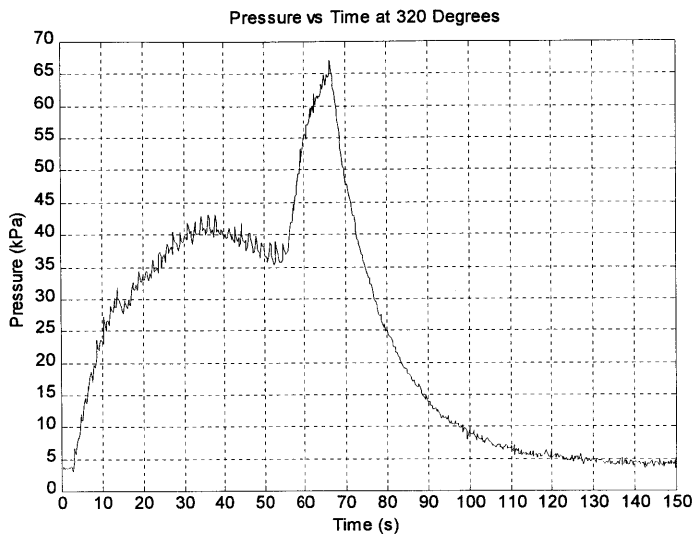


Figure 66. Pressure vs. Time Relationship at 320 Degree Location

The goal of the internally pressurized leakage experiment was to relate internal pressure to initiation of leakage. This was qualitatively achieved but is still lacking the accurate measurement of oil film thickness. Here only estimations may be evaluated to correlate theory to experiments. In its most basic form, the model of Chapter 2.3 can be used by a seal designer to ensure that initial waviness is not to large so as too promote leakage. This experiment and model also provide insight into the limitations of pressurization for a face seal.

# Chapter 5

# Discussion

In this section, detailed comments on experimental results and modeling will be presented in regards to the surface wave features of face seals. The following discussions will be presented in the same format as Chapters 2 and 4. Issues related to the deflection of surface waves will be presented first, followed by a discussion of hydrodynamic lubrication testing, and concluded with a discussion regarding internal pressurization versus leakage of a face seal.

## 5.1 Surface Wave Deflections

During this experiment the use of static LIF was very important in obtaining qualitative results. By imaging statically rather than dynamically, results were not complicated by torsional and thermal distortions in the seal geometry or by fluorescence signal degradation due to excessive heating. Static imaging left only laser intensity fluctuations and associated camera and signal noise as issues. One noise source characteristic of the 12 bit digital camera is known as dark current. Dark current is a phenomenon resulting from the thermal noise associated with the camera, and is easy to measure and eliminate. One can physically measure the amount of dark current by placing a lens cover on the digital camera and capturing an image. The black image obtained should have light levels equal to zero. With dark current however, the values of the light levels can be substantially higher (measured values for a Princeton Instruments RTE/CCD-1300 12 bit Scientific Camera were in the range of 120-160 pixel intensity). If fluorescent light levels of the oil film are on the same order of magnitude as the dark current, misleading results may be obtained. Dark current can corrected for by calculating the average pixel intensity in the lens cover image and subtracting this from the desired LIF image.

Results presented in Figure 37 are a result of using the LIF technique to produce a qualitative representation of the surface wave deflections. In a sealing application this static instability may lead to inconsistent wear and unpredictable deformed geometry, which may hinder hydrodynamic performance. Although not evaluated (experimentally), it is believed that a design of at least three periodic surface waves would allow a more consistent prediction of the surface deflections. By increasing the number of waves it can be seen from Figure 10 in Chapter 2.1a, that the seal will resist deformation at the higher loadings by 10%. This additional stiffness must be compensated in a hydrodynamic design which is sensitive to the surface wave geometry.

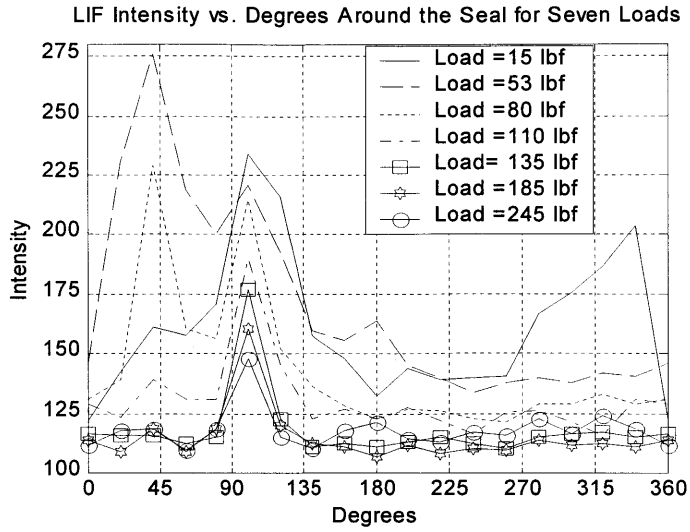


Revisited Surface Wave Deflection Plot Chapter 4.1, Figure 37.

It should be noted that the analysis does not take into consideration structural rotations. In addition, the geometry is assumed to be a perfectly parallel sinusoidal wave. This is not necessarily true for the seal used in the experiment. Figure 37 shows that there is a slight taper present in the seal. This taper would allow the outside edges of the seal under the crests of the waves to come into contact first. The analysis may not reflect the non-linear behavior of the experiment because the structural deflections were neglected for the analysis.

Analyses performed did not consider deflections caused by hydrodynamic pressure generation, sliding forces while in boundary lubrication, or thermal distortions due to viscous or interfacial friction. When these concepts must be employed to more accurately correlate experimental data to the models, the development process becomes increasingly complex. This is typically known as Thermo-Elasto-Hydrodynamic Lubrication modeling (TEHL) (Lebeck [3]).

## 5.2 Surface Wave Lubrication

Evaluation of lubrication was performed using two separate experiments, the first of which was covered in Chapter 4.2, on the effect of surface wave amplitude on hydrodynamic load support. The second was to help evaluate the effect of the laser engraved markings on lubrication. This was conducted as a control and sample experiment to evaluate if the engravings affected lubrication. If no significant changes were found, then the technique of placing laser engraved numbers would provide an inexpensive method of position information when used in conjunction with LIF.

The first experiment attempted to sort out the effect of wave amplitude on lubrication. Due to a rather small sample of production face seals (quantity = 40 seals), CMM surface geometry data revealed that the largest range of wave height to perform a comparison study was between 8 μm and 20 μm. Hydrodynamic theory of Chapter 2.2 revealed that these seals would have similar behavior with regard to load support. Behavior of both seals was very similar. The only parameter which did not agree between the two seal experiments was that of the f-G plots of Figures 47 and 48 shown below.

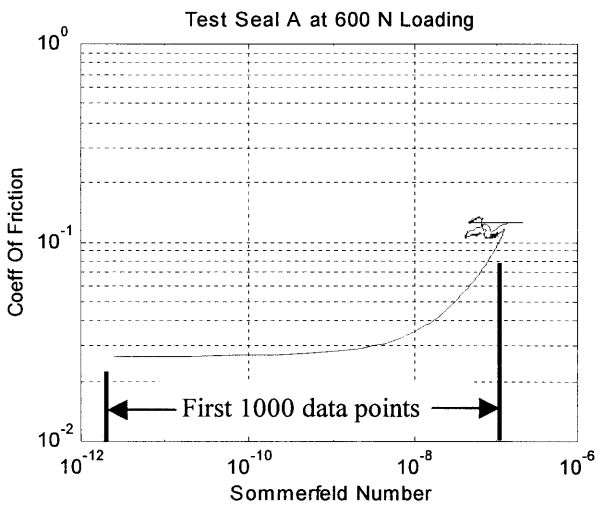


Revisited Figure 47. f-G Plot for Seal A at 600 N

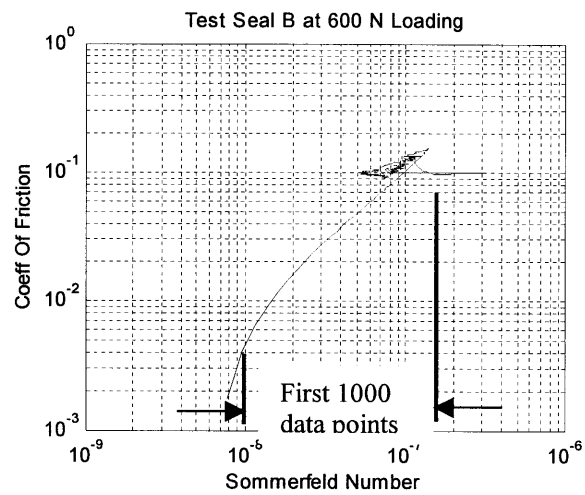


Revisited Figure 48. f-G Plot for Seal B at 600 N

Here it can be seen that the trend of f-G in Test Seal A is drastically different from Test Seal B. It should be noted that the data set consists of 48,000 data points taken across 6.7 hours. The major difference in data between Figure 47 and Figure 48 takes place across the first 1000 points, or 8 minutes of operation.

Correlation of theory to experiments for the wave amplitude experiment was presented in Chapter 4.2. Although agreement was not evident, a new insight was gained in the theoretical modeling associated with this problem. This insight was that

quantitative film thickness measurements will be necessary to verify the current models. Quantitative film thickness would aid in understanding the relationship between asperity load support and hydrodynamic load support. This will aid in the establishment of an appropriate lubrication model for the face seal.

The second experiment involved a comparison of two seals that were identical with the exception the laser-engraved numbers on one of the seals. This experiment was designed to determine if the laser engraved markings affected lubrication in a significant manner. Both seals were subjected to the operating conditions described in Chapter 4.2. A dramatic result with regard to seal temperature was observed. Figures 69 and 70 present the temperature results from these experiments. A 50 degree Celsius reduction in maximum seal temperature for the laser engraved seal was observed for the high (600 N) load condition. The region of the engravings is located in a rather thick oil film (0.5 mm). Previously this region of the was thought to have no influence on lubrication.

An experiment to validate this result was conducted and results showed that there was no temperature reduction between engraved and non-engraved seals. An exact duplication of the results of Figure 70 was not possible due to a limited supply of 192mm laser engraved seals. This validation experiment used a 92mm diameter seal. The seal used for the results discussed above (presented in Figure 70) was 192mm in diameter. Future research should attempt to verify the results of Figure 70 and classify these results as an anomaly or fact.

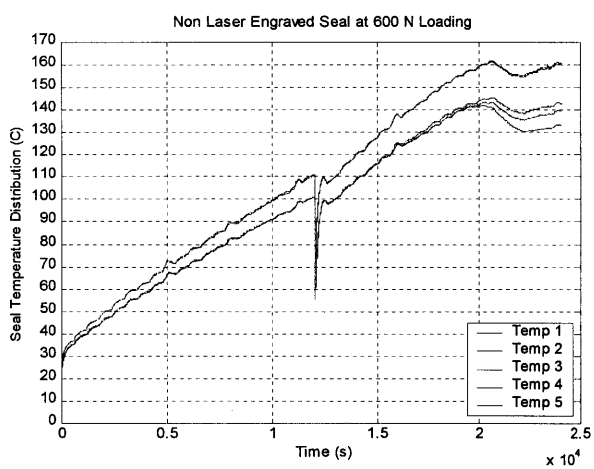


Figure 67. Non-Laser Engraved Seal Temperature Results

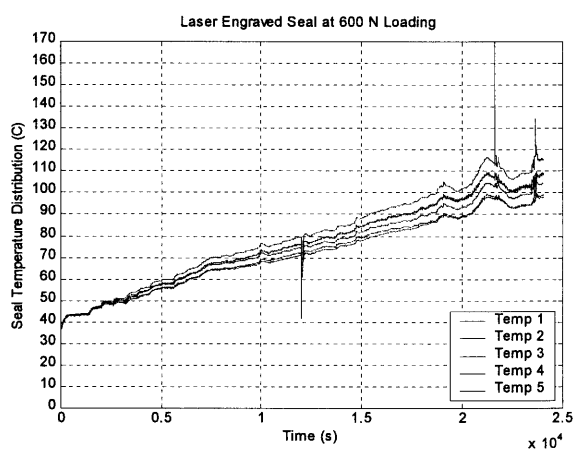


Figure 68. Laser Engraved Seal Temperature Results

Correlation to experimental results was not successful in proving the hydrodynamic theory developed from Chapter 2.2. Currently, proper evaluation of the theory cannot be made due to

the inability to obtain quantitative film thickness data. Model characterization can only be made once film thickness is known. Current operation of the face seal may be predominately boundary lubrication. If boundary lubrication is prevalent, the theory presented would not be applicable. To date, quantitative dynamic film thickness measurements have not been achieved. Development of a calibration technique for LIF is difficult and particular to the experiment at hand. Once completed, LIF will provide experimentalists with a powerful tool for extracting 3-D film thickness and flow visualization in tribiological applications.

### 5.3 Internal Pressurization

It was demonstrated in Chapter 4.3 that a seal of a 8μm gap height could not sustain internal pressures greater than 5-40kPa (0.5-6 psi). This agrees with theory based on a pressure balance utilizing surface tension. LIF provided a means to visually evaluate the onset of leakage. As described in Chapter 5.2, the extraction of quantitative values of film thickness would provide a more solid foundation when comparison to theory is presented. This analysis does show that face seals of this construction cannot support large internal pressures.

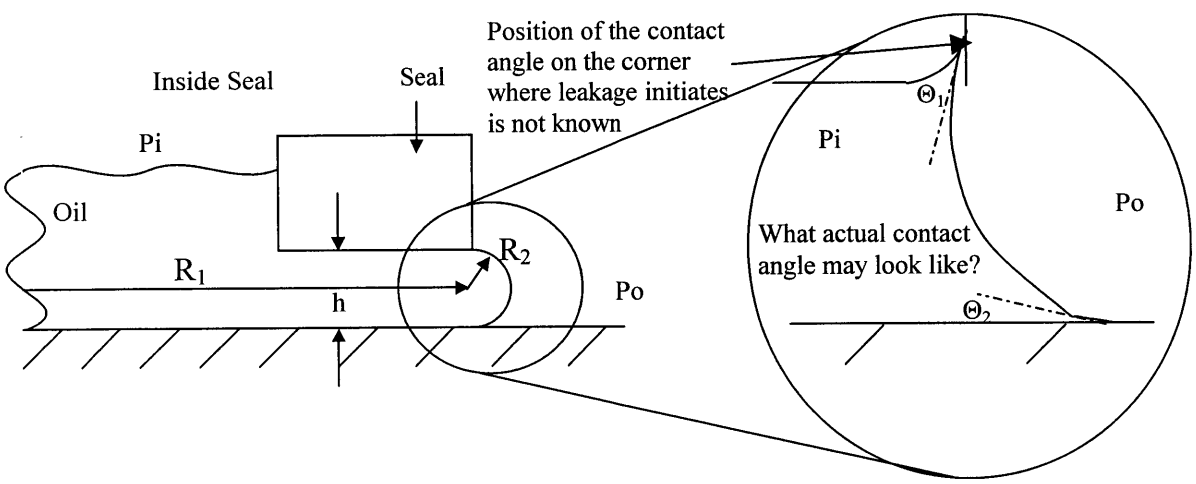


Figure 69. Contact Angle Illustration.

The surface tension analysis presented in Chapter 2.3 provided an estimation of the maximum value of gap height that will initiate leakage given an internal pressure. The analysis considers that the entire surface tension force acts in the direction opposite of the leakage. This statement ignores the actual contact angle at the interface and imposes an angle of 180-degrees. The actual contact angle of the fluid/surface interface is a measurable quantity but the difficulty arises in at what position the film ruptures. An understanding of surface tension/contact angle mechanics is required to obtain a more accurate relationship between the internal pressure and gap height. The analysis presented in Chapter 2.3 provides an upper bound solution to this problem.

# Chapter 6
# Conclusions

An investigation of the tribiological effects of surface wave geometry using LIF and traditional measuring techniques has been presented. The importance of such features to hydrodynamic load support is supported by the growing amount of ongoing research in the field. Seal manufacturers can greatly benefit from a firm understanding of the factors that affect lubrication and what can be done to enhance performance.

Through the use of LIF, it has been demonstrated that surface deflections can be characterized by Hertzian contact mechanics. It was presented in Chapter 2 that increasing wave amplitude and increasing the number of waves of a face seal increases seal stiffness. Experimental deflection of a face seal surface wave was evaluated using LIF and showed a strong correlation to the model developed in Chapter 2.1.

Modeling of hydrodynamic lubrication of a face seal surface wave was presented in Chapter 2.2. Trends in modeling results correlate to the assumptions presented. It was discovered using a hydrodynamic lubrication model based on Reynolds equation that there lies an optimum wave amplitude for maximum load support. In addition, it was discovered that for a small number of surface waves (<3 waves) load support is proportional to the number of waves present. After three surface waves, load support begins to diminish to a constant value, thereby showing limitations of increased number of surface waves present on a seal.

Experimental comparison to the theoretical findings of Chapter 2.2 was not conclusive. This comparison was accomplished using theoretical and experimental data in regards to coefficient of friction versus Sommerfeld Number. Experimental trends suggest that the face seal operates in the hydrodynamic regime. Experimental results of the coefficient of friction range from 0.1 to 0.2 and Sommerfeld Number ranges from $4*10^{-7}$ to $10^{-6}$. Theoretical predictions show very low values of the coefficient of friction (0.02 to 0.1) across Sommerfeld Numbers of $10^{-8}$ to $10^{-6}$. These results indicate that full hydrodynamic modeling may not be appropriate. A mixed friction model of lubrication considering asperity interaction may provide stronger correlation to the experiments presented.

Through the use of LIF it was possible to show how internal pressurization of the face seal induced leakage at low pressures. Leakage was qualitatively evaluated by observing the progression of the meniscus present at the outer diameter of the face seal/quartz interface. Pressure at which leakage occurred correlated well with theoretical predictions based on surface tension. Modeling demonstrated the necessity of small gaps between seal surfaces if much larger internal pressures are desirable.

Research presented has provided a means of lubrication visualization through the use of Laser induced Fluorescence, which previous investigators have often neglected. Once perfected, these optical diagnostic techniques will prove to be invaluable to tribologists. Future research should build upon techniques and concepts presented in this thesis. Further development of the seal models presented in Chapter 2 is required in order to obtain a means of accurate prediction of the seal behavior for the experiments. The ultimate goal is to have a solid understanding of the underlying physics behind the lubrication of face seals and to apply this knowledge to existing and new face seal designs.

# Chapter 7
# Future Work

***Surface Wave Deflection Experiment***

There is room for improvement in both modeling and experimentation. Modeling should be reconsidered using a two-dimensional discretized version of Hertz's Equation. This would allow the implementation of real geometries incorporating taper of the contact interface. In addition, it would be advantageous to incorporate a model based on structural rotations of the cross section. Correlation of the deflection experiments to theory in Chapter 4.1 did not consider these structural rotations. Future research may consider developing a model using a commercial FEA package such as COSMOS [23].

The surface wave deflection experiment should be repeated in finer degree increments. The resolution of Figure 40, Chapter 4.1 would be dramatically increased with finer image spacing, (5-10 degree).

Face seals used for such an experiment should have a minimum of three surface waves of equal amplitude. This may reduce error incurred from tilting of the seal which was speculated in results presented in Chapter 4.1.

***Wave Amplitude Lubrication Experiment***

The model should be reconsidered using a mixed-friction model that takes into consideration the interaction of asperities and their contribution to load support (Lebeck [3]). In addition, cavitation may play an important role in the theoretical modeling. There exists regions of the seal that in operation may produce low pressure regions which may initiate cavitation. These effects were not considered for the comparison but have been investigated by Lebeck [3], Salant and Payvar [20], Nau [12], and Elrod [21]. These studies have shown that this phenomenon has a strong influence on results of lubrication models.

For an experimental comparison, a face seal with virtually no wave amplitude less than 1 μm should be constructed and evaluated for performance. If theoretical predictions of Chapter 2.2c are correct, the seal would not produce significant load carrying capacity at moderate speeds (<6m/s). Several seals should also be produced and evaluated with increasing wave amplitude. If modeling applied in Chapter 2.2c agrees with experimentation, there should lie an optimum wave amplitude for a given speed, viscosity, etc, see Figure 17. These experiments would greatly aid in seal design. Obtaining face seals of these specifications may be difficult due to issues related to the manufacturing of defined surface features of less than 50 μm in dimension.

***Leakage Experiment***

Development of the model and experiment should be applied to rotating seal applications. It is apparent that face seals under static conditions cannot sustain very high internal pressures if the gap is on the order of a few microns. One means of keeping a wavy seal from leaking would be to externally pressurize the seal to balance internal forces on the fluid. Another possibility is to include reverse pumping grooves as suggested by Salant and Homiller [22] to retain lubricant and prevent leakage. In addition, temperature effects related to surface tension and leakage should be investigated due to the extremely high temperatures observed in Chapter 5.2.

***Experimental Procedure Overview***

Future modeling should attempt to couple hydrodynamic pressure generation with structural deformation (Lebeck [3]). This analysis would lead to increased solution time due to model complexity. As computational power continues to increase for desktop PC's this will become a lesser issue in years to come.

Future investigation should continue into the development of LIF for quantitative film thickness data. This will provide direction for theoretical modeling. Until quantitative values can be assigned to LIF images, justification for modeling assumptions can only be supported by results of previous investigators and trends observed in experimental results.

***Experimental Test Rig***

There is much room for improvement in regards to the experimental test rig used for this research. A more reliable method of face seal fixturing needs to be developed. The current apparatus allows the seals to wobble at high rotational speeds. In addition, the 92 mm seals tested at high speeds produced so much centrifugal acceleration that much of the oil was lost due to spraying out from the thermocouple probe locations. This was detrimental to the operation due to excessive heating and eventual scoring of the quartz.

In order to validate the theoretical models developed, it is necessary to mount the seal face a fixed distance from the secondary mating surface. This would eliminate the zero film thickness assumption. Normal load readings would then be representative of hydrodynamic lift associated with the flow. Mounting would need to be controlled to compensate for thermal expansion of the system due to viscous heating. This would provide a more controlled environment for a comparative study.

Quartz plates used for experiments were modeled as perfectly flat plates. It was discovered very late in this research that quartz plates used have as much waviness as the face seals being investigated. The use of thick optical flats should be considered so as to have an experiment which is closely coupled with the theory developed.

Motor controls in current test rig do not allow the motor to be easily reversed. This is necessary for evaluation of the seals in both directions. Many metal face seals experience bi-directional operation.

During experiments it was noticed that a considerable amount of noise was induced into the normal face load and torque signals. These sources of error were not accounted for and were suspected to reside in the transducers selected. Future experiments should utilize a high precision combination force/torque transducer mounted to the quartz plate-retaining fixture.

The ability to capture leakage would provide additional data to help correlate theoretical models. Lebeck [24] describes a clever technique of leakage data collection. This consists of a accumulation device set to trigger at 2.5 ml increments. The same approach could be taken with a more modern electronic balance with data communication possibilities. This would allow an easy interface to current data acquisition equipment available.

**References:**


1. Young, LA, Lebeck, AO, "The Design and Testing of a Wavy-Tilt-Dam Mechanical Face Seal", Lubrication Engineering, Vol 45, May 1989, 322-329.
2. Etsion, I, Michael O, "Enhancing Sealing and Dynamic Performance with Partially Porous Mechanical Face Seals", Tribology Transactions, Vol. 37, no. 4,Oct. 1994, 701-710.
3. Lebeck, AO, 1991, "Principles and Design of Mechanical Face Seals", Wiley, ISBN 0-471-51533-7.
4. Lebeck, AO, "Hydrodynamic Lubrication and Wear in Wavy Contacting Face Seals", Journal of Lubrication Technology, Vol 100, January 1978, 81-91
5. Lebeck, AO, United States Patent Number 4,836,561, "Wavy-Tilt-Dam-Seal Ring",1989
6. Lebeck, AO, United States Patent Number 4,973,068, "Differential Surface Roughness Dynamic Seals and Bearings",1990
7. Lebeck, AO, United States Patent Number 4,887,395, "Wavy-Tilt-Dam-Seal Ring and Apparatus for Shaping Seal Rings",1989
8. Young, LA, Lebeck, AO, "The Design and Testing of a Moving Wave Mechanical Seals Under Variable Operating Conditions in Water", Lubrication Engineering , Vol 42, no 11, Nov. 1986, 677-685.
9. Etsion, I, Kligerman Y, "Analytical and Experimental Investigation of Laser Textured Mechanical Face Seals", Tribology Transactions, Vol. 42, no. 4,Sept. 1999, 511-516.
10. Etsion, I, Burstein L, "A Model for Mechanical Face Seals with a Regular Microsurface Structure", Tribology Transactions, Vol. 39, no. 3,Sept. 1996, 677-683.
11. Green, I, Insolia, G, "Design Modeling, and Animation of Non Contacting Mechanical Face Seals", Lubrication Engineering ,Vol 47, April 1991, 189-190.
12. Nau BS, "Film Cavitation Observations in Face Seals", Proceedings of the 4th International Conference on Fluid Sealing, BHRA, Paper No. 20, 1969, 205-217.
13. Johnson, KL, 1985, "Contact Mechanics", New York , Cambridge University Press, ISBN 0521255767
14. Sabersky, R.H., Acosta, A.J., 1964, "Fluid Flow: A first Course in Fluid Mechanics", Macmillan, NewYork, NY
15. Seireg, A., 1998, "Friction and Lubrication in Mechanical Design", New York, Marcel Dekker, ISBN 0824799747
16. Cameron, A, 1966, "Principles of Lubrication", Wiley, New York, NY

**References:**

17. Taylor, R.I., "The inclusion of Lubricant Shear Thinning in Journal Bearing Models", Proceedings of the 25th Leeds-Lyons Symposium on Tribology, Lyon France, Sept. 1998
18. Hidrovo, C.H, Hart, D.P, "Dual Emission Laser Induced Fluorescence Technique (DELIF) for Oil Film and Temperature Measurement", Proceedings of the ASME FEDSM 2000, Paper no. 1, June 2000
19. Brown and Sharpe, April 2000, http://www.brownandsharpe.com/products/inedx.html
20. Salant, R.F. Payvar, P., "A Computational Method for Cavitation in a Wavy Mechanical Seal", Journal of Tribology, Vol. 114, Jan 1992, 199-204
21. Elrod, H.G., "A Cavitation Algorithm", Journal of Lubrication Technology, Vol. 103, July 1981, 350-354.
22. Salant, R.F., Homiller, S.J., "Effects of Shallow Groove Patterns on Mechanical Face Seal Leakage", Tribology Transactions, Vol. 35, no. 1, Jan 1992, 142-148
23. COSMOS FEA, April 2000, http://www.cosmosm.com
24. Lebeck, A.O., "Test Apparatus for Measuring the Effects of Waviness in Mechanical Face Seals", ASLE Transactions, Vol 24, No 3, 1981, 122-128.
25. OMEGA, April 2000, http://www.omega.com/pressure/

## Appendix A

Explanation of Programs used for Face Seal Research:

*FaceSeal_fig.m* allows the user to access the raw data in comma separated or tab delimited form and plot the results of a Face Seal Experiment. In addition *FaceSeal_fig.m* provides access to other analysis programs developed for this research. All results are plotted in SI units.

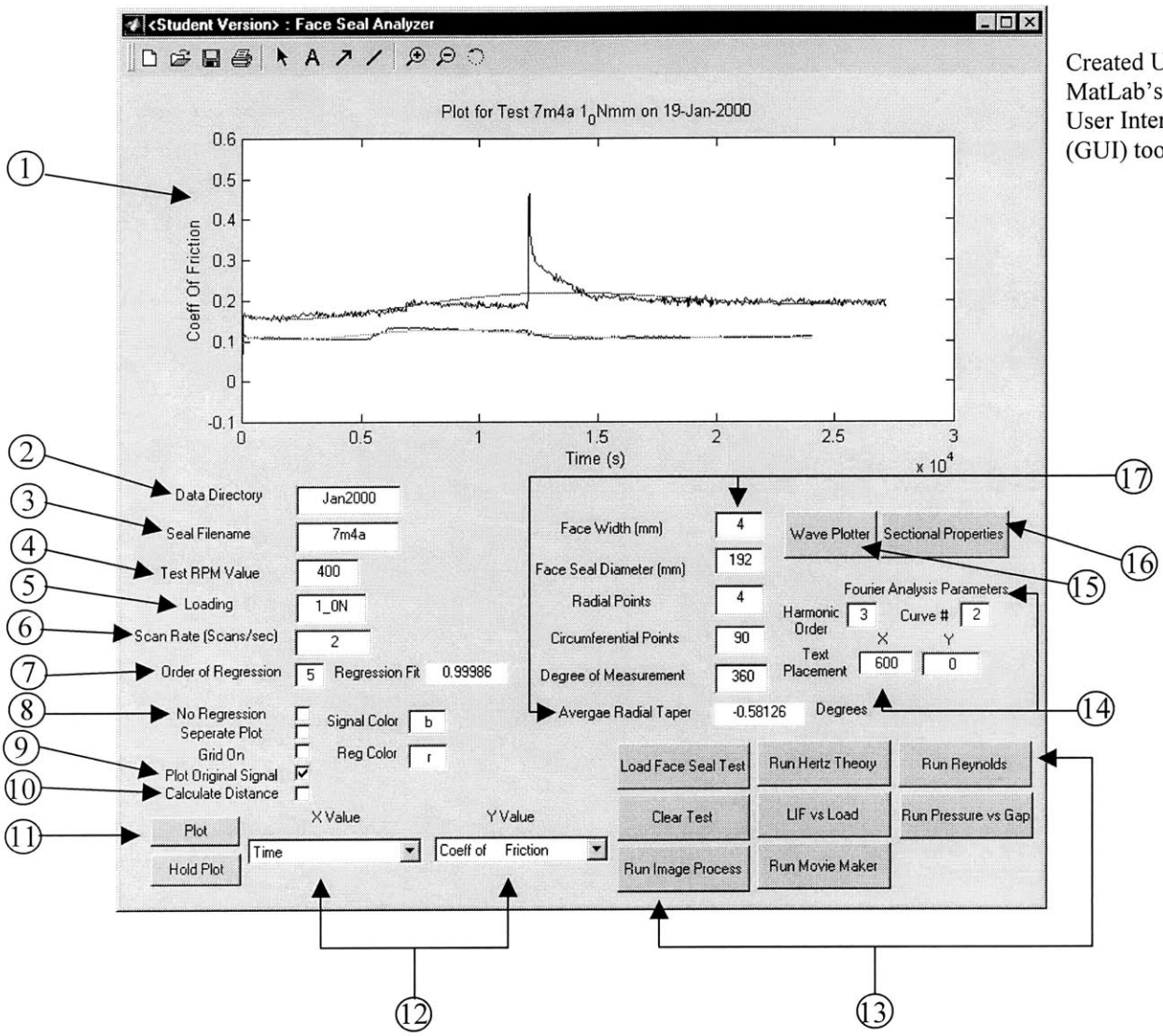


Created Using MatLab's Graphical User Interface (GUI) toolbox

Programs called by *FaceSeal_fig.m*

*FaceSeal_fig.mat*
*arrow.m*
*CrossSection.m*
*fourier.m*
*File2Var.m*
*Plotter.m*
*RingProp.m*
*Taper.m*
*Hertz.m*
*waveplotter.m*
*reynolds.m*
*extract.m*

Numbered Explanation of Program *FaceSeal_Fig.m*

1. **Viewable Plotting Area**.
2. **Data Directory**; This is provided in order for the program to switch directories to find the required data.

   Required Directory Structure.

   e:\george\matlab\testdata\[*Data Directory Name Here*]\[*Seal Filename Directory Here*]

   Example: e:\george\matlab\testdata\jan2000\7m4a

   **Note: Programs required for proper operation of *FaceSeal_fig.m* should be installed in *e:\george\matlab* directory including *FaceSeal_fig.m.* Once the MatLab environment has started, at the prompt type cd e:\george\matlab and press "Enter", now type *FaceSeal_fig.m* and the above Figure will appear. If the user does not use the directory *george* then all programs which use this format must be changed to accommodate the desired directory name.

3. **Seal Filename**; Item 2 of this list shows the use of a " [*Seal Filename Directory Here*]". In this location the filename is used for the directory name. Place the seal data file in this directory using the structure;

   Test_[*Seal Filename Directory Here*]_[Loading Format Here]_mm.m

   **Note: "Test_" is placed in front of the data file name to prevent MatLab from trying to convert the numeric filenames to numeric digits.

   Example: *Test_7m4a_1_0N_mm.m*

   The format of the data file may be tab delimited or comma separated.

4. **Test RPM Value**; Enter the RPM at which the experiment took place.

5. **Loading**; Entry provides data for the [Loading Format Here] field in Item 3. In addition the seal data filename should be formatted with the loading criterion used such as the example provide in Item 3.

   **Note: The loading criterion used in this thesis was 0_#N, which corresponds to 0.# Newton per millimeter circumference of the face seal.

   Example: For 1.0N/mm loading use 1_0N in the data field.

6. **Scan Rate**; Enter the Sampling Rate of the acquisition for the particular experiment to be analyzed.

7. **Order of Regression**; Select the desired order of regression to be used for a given plot. "$R^2$" value of the curve fit will be updated for every graph where regression has been applied.

8. **No Regression**; Select this check box to not plot the curve fitted data.

9. **Plot Original Signal**; Select this check box to plot the original sampled data.

10. **Calculate Distance**; Select this check box when it is necessary to calculate the distance traveled of the face seal surface.

    **Note: When this option is selected initial data extraction is slow. It is recommended to be turned off when distance traveled is not desired.

11. **Plot**; Press this button to plot what is highlighted in the text fields of Item 12.

12. **Pull Down Variable Menus**; Variables from an experiment may be plotted on the X or Y axis by selecting the corresponding menu location. The following variables are listed as options:

| | |
|---|---|
| *Time for Temp and Dynamic Viscosity* | *Temp 3* |
| *Speed* | *Temp 4* |
| *Time* | *Temp 5* |
| *Torque* | *Temp 6* |
| *Face Load* | *Seal Temperature Distribution* |
| *Coefficient of Friction* | *Calculated Film Thickness based on Couette Flow* |
| *Dynamic Viscosity* | *Sommerfeld Number* |
| *Temp 1* | *Power Dissipation* |
| *Temp 2* | *Distance Traveled* |

13. **Push Buttons Calling Other Programs**; Functions are called from these buttons that correspond to the other programs described in this thesis.

    **Note: Pressing the button labeled "Load Face Seal Test" will load the data in the file referenced in Item 3. The format of the data file to be used by this program is;

| Speed(Rpm), | Torque(in-lbf), | Normal Load (lbf), | Temp 1 (C), | Temp 2 (C), | Temp 3(C), | Temp 4(C), | Temp 5(C), | Temp 6(C) |
|---|---|---|---|---|---|---|---|---|
| #, | #, | #, | #, | #, | #, | #, | #, | #, |
| #, | #, | #, | #, | #, | #, | #, | #, | #, |
| #, | #, | #, | #, | #, | #, | #, | #, | #, |
| #, | #, | #, | #, | #, | #, | #, | #, | #, |
| #, | #, | #, | #, | #, | #, | #, | #, | #, |
| #, | #, | #, | #, | #, | #, | #, | #, | #, |

**Note: Only Numeric values separated by commas are to be used in the face seal experiment data file of Item 3.

Deviation from this format will result in errors.

14. **Fourier Analysis Text Placement feature**; Displays the results from a Fourier analysis of face seal waviness data obtained from a CMM machine.

    **Note: CMM Waviness data should be formatted in the following form;

$$\left.\begin{array}{ccc} X_1, & Y_1, & Z_1, \\ X_2, & Y_2, & Z_3, \\ . & . & . \\ . & . & . \\ . & . & . \\ . & . & . \\ X_N, & Y_N, & Z_N, \end{array}\right\} \text{1}^{\text{st}} \text{ Circumferential Trace, O.D. of Face Seal}$$

$$\left.\begin{array}{ccc} X_1, & Y_1, & Z_1, \\ X_2, & Y_2, & Z_3, \\ . & . & . \\ . & . & . \\ . & . & . \\ . & . & . \\ X_N, & Y_N, & Z_N, \end{array}\right\} \text{2}^{\text{nd}} \text{ Circumferential Trace, Moving from O.D. to the I.D. of the Face Seal}$$

    Where N is the number of circumferential data points taken in one circular trace.

    Deviation from this format may result in erroneous waviness plots.

15. **Wave Plotter**; Push Button which calls the program which reads the seal waviness file and plots the results.

    Format of the seal waviness data filename should be:

    s[*Seal Filename Directory Here*].m

    **Note: "s" is placed in front of the data file name to prevent MatLab from trying to convert the numeric filenames to numeric digits.

    Example: *s7m4a.m*

    The program uses the text field of Item 3 to locate the waviness data.

16. **Sectional Properties**; Push Button which calls the program which reads the seal cross sectional data file and plots the results.

    Format of the seal cross sectional data filename should be:

    s[*Seal Filename Directory Here*]profile.m

    **Note: "s" is placed in front of the data file name to prevent MatLab from trying to convert the numeric filenames to numeric digits.

    Example: *s7m4aprofile.m*

The program uses the text field of Item 3 to locate the seal cross sectional data.

**Note: Cross sectional measurements may be taken using a CMM machine. The seal should be oriented so that the cross section lies in the Y-Z plane. The program will not calculate the cross sectional properties if the data is not in this form. Cross sectional data should be formatted in the following form;

$$
\begin{array}{lll}
0, & Y_1, & Z_1, \\
0, & Y_2, & Z_3, \\
. & . & . \\
. & . & . \\
. & . & . \\
. & . & . \\
0_N, & Y_N, & Z_N,
\end{array}
$$

17. **Waviness Plotting Options**; Enter here the format of the waviness measurements; these parameters are used by Item 15.

*ImageProcess.m* allows the user to access the LIF images. Manipulation of the image can be performed to highlight particular characteristics. This program requires having MatLab v.5.3 with the Image Processing toolbox installed. *ImageProcess.m* is called from *FaceSeal_Fig.m* and resides in the directory "images". The following directory structure is required:

e:\george\matlab\images

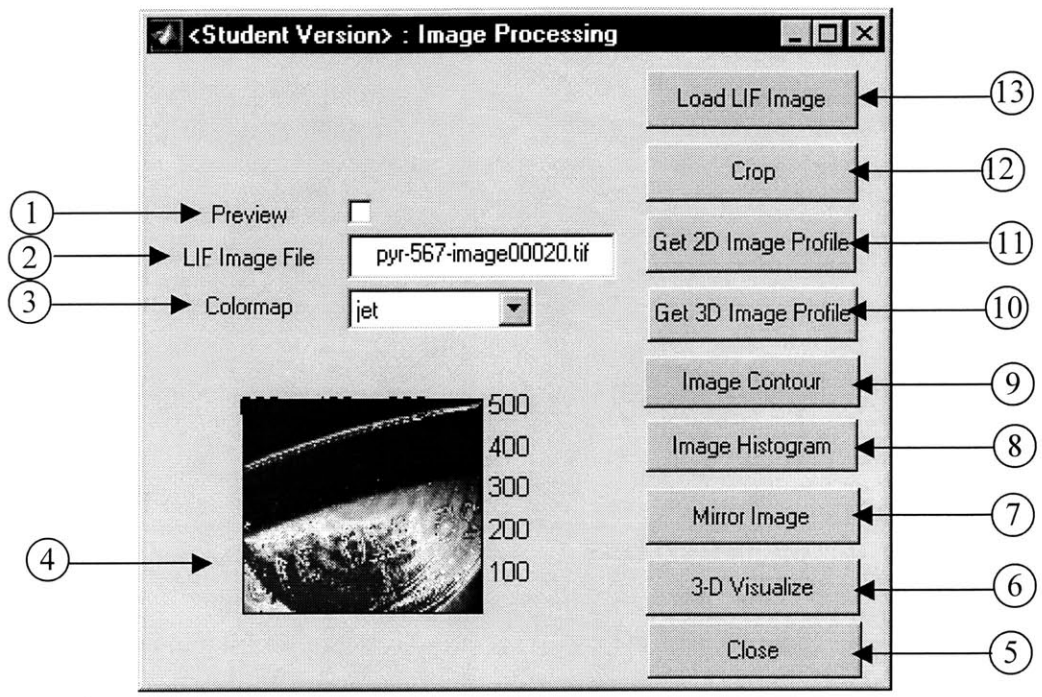


Programs called by *ImageProcess.m*

*ImageProcess.mat*
Image Processing toolbox of MatLab v.5.3

Numbered Explanation of Program. *ImageProcess.m*

1. **Preview Check Box;** Selection this option when a preview of the image is desired. The preview is displayed in the graphical user interface.

2. **LIF Image File**; Location to enter the image filename.

3. **Colormap;** Changes the associated color scheme of the image to be processed.

4. **Preview Image Location;** Location where the image can be previewed by selecting Item 1.

5. **Close Button;** Pressing this button closes the program and returns to the associated face seal directory of *e:\george\matlab.*

6. **3-D Visualize;** Function which converts current image to 3-dimensional data representation which highlights the low signals in the image by inverting each pixel value.

7. **Mirror Image;** Produce a left to right flip (mirror) of the current image.

8. **Image Histogram;** Function to calculate a histogram of the current image. This function provides a distribution of intensity values in the image.

9. **Image Contour;** Function which takes the current image and generates a contour map representation.

10. **Get 3-D Image Profile;** Function which allows a multipoint pixel trace in the current image window. Pressing enter completes the trace and plots the pixel intensity values in a 3-D representation.

11. **Get 2-D Image Profile;** Function which allows a line pixel trace in the current image window. Pressing enter completes the trace and plots the pixel intensity values in a 2-D representation.

12. **Crop;** Perform a rectangular crop of the current image. Image data is reformatted and plotted in the same window.

13. **Load LIF Image;** Function which loads and formats the selected image data in a figure window.

*Hertz.m* allows the user to perform theoretical Hertz contact mechanics analysis for a 1-D surface wave. Analysis presented in Chapters 2 & 4 were performed using the files *Hertz.m* and *HertzTheory.m*

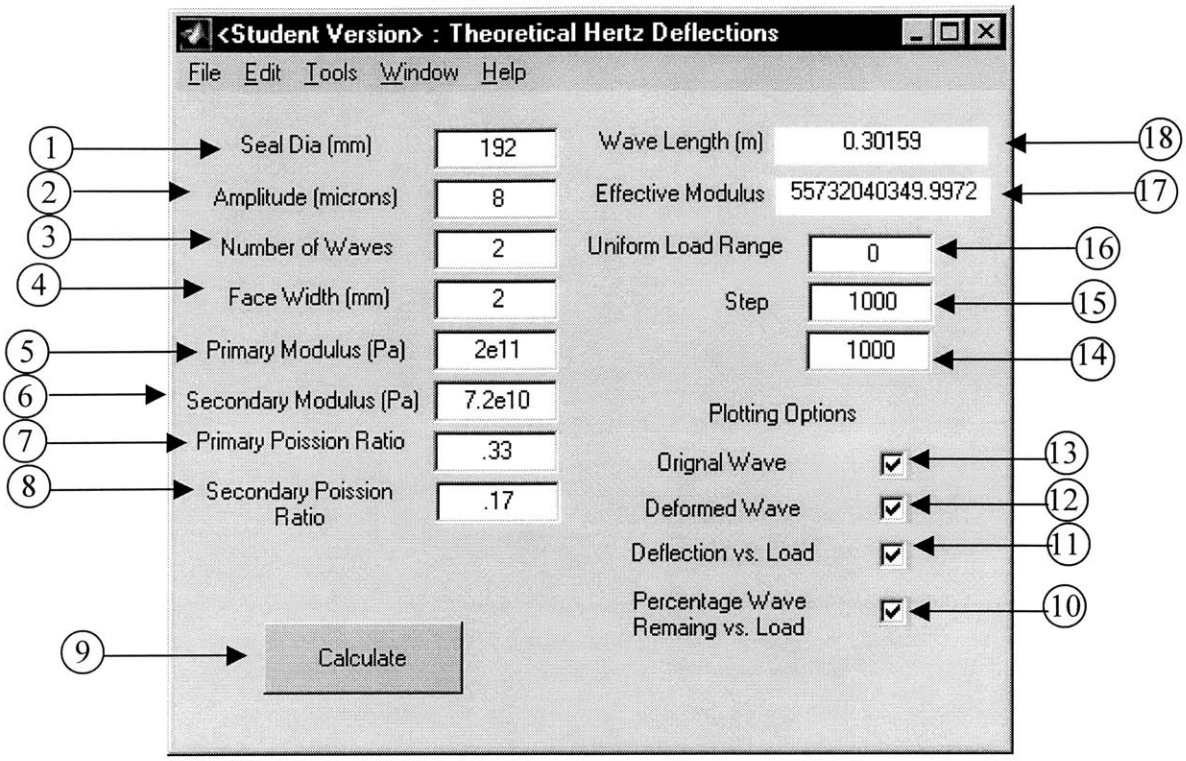


Programs called by *Hertz.m*

*Hertz.mat*
Image Processing toolbox of MatLab v.5.3

Numbered Explanation of Program *HertzTheory.m*

1. **Seal Diameter;** Enter the diameter of the seal in mm.

2. **Amplitude;** Enter the face seal surface wave amplitude in microns.

3. **Number of Waves;** Enter the number of load supporting wave crests.

4. **Face Width;** Enter the face seal face width in mm.

5. **Primary Modulus;** Enter the modulus of elasticity of the face seal material.

6. **Secondary Modulus;** Enter the modulus of elasticity of the mating surface material (Quartz), (Pa).

7. **Primary Poisson Ratio;** Enter the Poisson ratio of the face seal material.

8. **Secondary Poisson Ratio;** Enter the Poisson ratio of the mating surface material (Quartz).

9. **Calculate;** Perform the specified anaylsis from Items 10 to 13.

10. **Percentage Wave load remaining versus Load;** Plot results of the Hertz Contact mechanics analysis. Items 1 to 8 and 14 to 16, govern the input parameters.

11. **Deflection versus Load;** Plot results of the Hertz Contact mechanics analysis. Items 1 to 8 and 14 to 16, govern the input parameters.

12. **Deformed Surface Wave ;** Plot the deformed surface wave geometry from the Hertzian Contact mechanics analysis. Items 1 to 8 and 14 to 16, govern the input parameters.

13. **Orignal Surface Wave ;** Plot the un-deformed surface wave geometry from the Hertzian Contact mechanics analysis. Items 1 to 8 and 14 to 16, govern the input parameters.

14. **Final Load;** Enter final value of the load applied to the seal geometry.

15. **Stepping Load;** Enter incremental value of the load applied to the seal geometry.

16. **Initial Load;** Enter initial value of the load applied to the seal geometry.

17. **Effective Modulus;** Calculation of the effective modulus (Equation 2) between the two face seal materials is computed and displayed here.

18. **Wavelength;** Wavelength of the face seal is computed and displayed here.

*LIFLoad.m* allows the user to extract surface wave deflection data from LIF experiments discussed in Chapter 4.1.The directory structure for the following program is.

e:\george\matlab\images

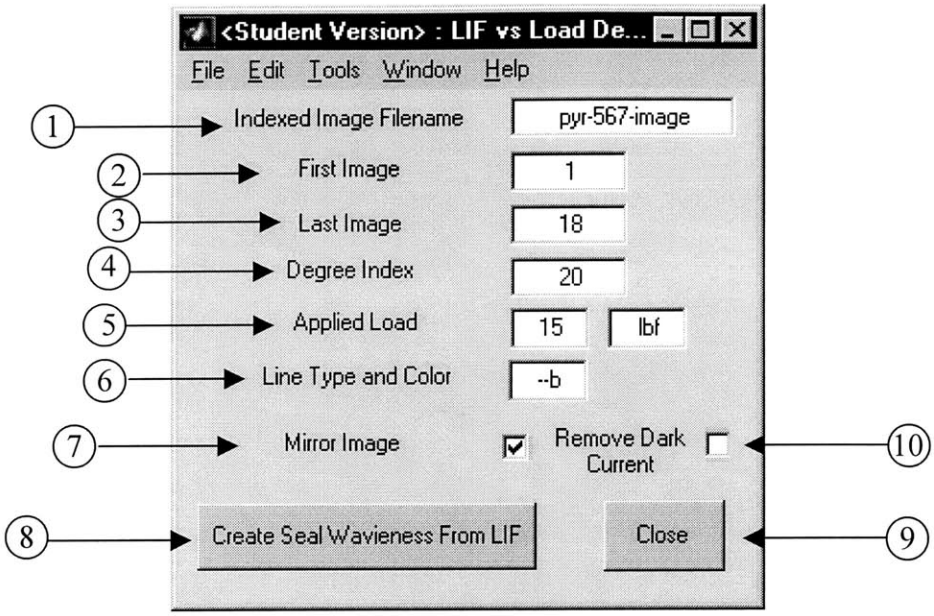


Programs called by *LIFLoad.m*

*LIFLoad.mat*
*LIFLoadDefl.m*
Image Processing toolbox of MatLab v.5.3

Numbered Explanation of Program *LIFLoad.m*

1. **Indexed Image Filename;** Enter the text only portion of the filename.

2. **First Image;** First Image in a experimental series.

3. **Last image;** Last Image in a experimental series.

4. **Degree Index;** Enter the angular spacing between images for plotting purposes.

5. **Applied Load;** Enter the applied load for title purposes.

6. **Line Type and Color;** Enter here the MatLab text strings representing different colors and lines types.

7. **Mirror;** Produce a left to right flip (mirror) of every image in the experimental data set.

8. **Create Seal Waviness from LIF;** Function which calls *LIFLoadDefl.m* which performs the extraction. Pressing this button will cause a window to appear with the first image loaded. The program is now waiting for a two point intensity profile to be drawn. This line should be drawn in the radial direction of the face seal and should only contain regions in the contact interface. Avoid drawing the profile across the meniscus or inner oil sump region. An example intensity plot region can be found in Figure 39, Chapter 4.1.

9. **Close;** Pressing this button closes the program and returns to the associated face seal directory of *e:\george\matlab.*

10. **Remove Dark Current;** Select this option when dark current from a digital camera is to be removed from a experimental data set. If dark current has been measured in the form of an image it must have the following filename.

    *darkcurrent.tif*

    **Note: When possible dark current values should be removed from the experimental data set. It was experienced by this author that neglecting to remove dark current values caused a 10% increase in observed face seal waviness under load.

    **Note: Filename structure can obtain any text string placed into Item 1. The filename should be structured as follows:

    *[Filename]XXXXX.tif*

    Where X is equal to numbers listed in Items 2 and 3. In the event the number does not contain 5 digits, pad the number as follows:

    Example. *pyr-567-image00001.tif*

*LIFMovie.m* allows the user to collect data from images of LIF experiments discussed in Chapter 4.2 and convert the data into .MPG formatted movies.The directory structure for the following program is.

e:\george\matlab\movies

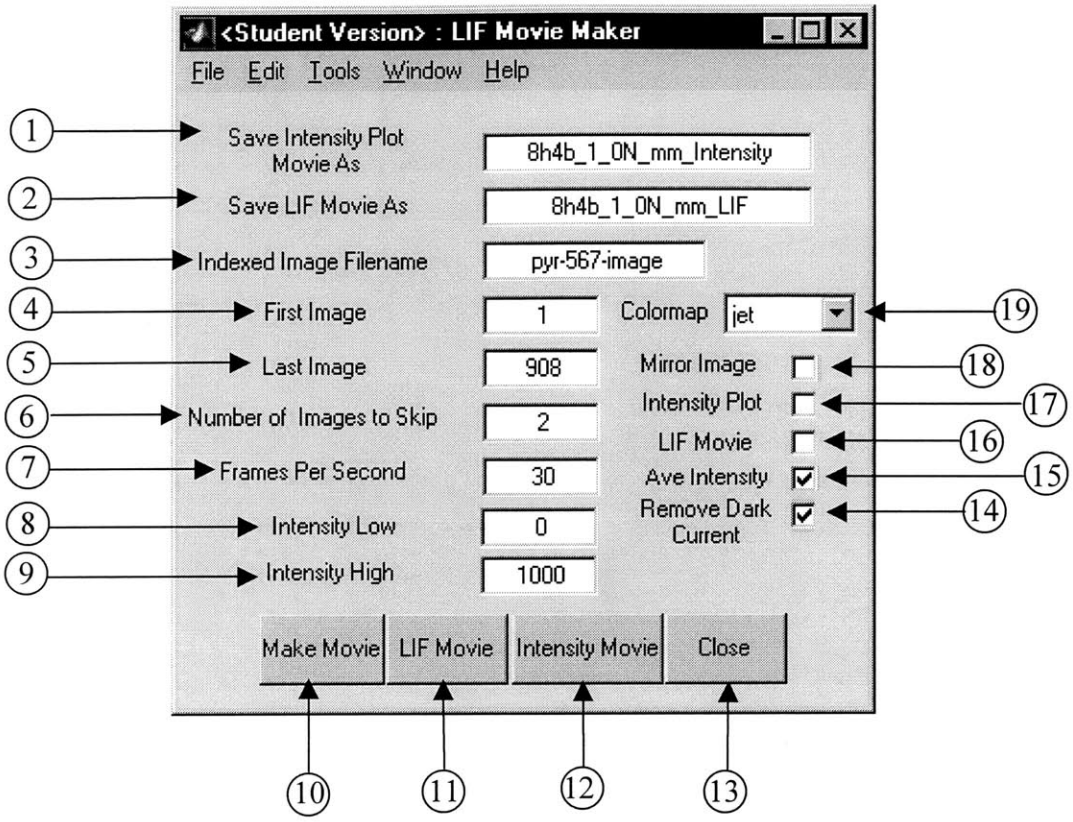


Programs called by *LIFMovie.m*

*LIFMoviemat*
*MovieMaker.m*
*Mpgwrite.m* (Obtained from the MatLab website www.matlab.com, comes with additional driver files)
Image Processing toolbox of MatLab v.5.3

Numbered Explanation of Program *LIFLoad.m*

1. **Save Intensity Plot Movie As;** Location to input the name of the LIF Intensity movie to be created and saved in a *Filename*.mpg format.

2. **Save LIF Movie As;** Location to input the name of the LIF movie to be created and saved in a *Filename*.mpg format.

3. **Indexed Image Filename;** Input the text portion of the filename from the LIF experiment to be viewed.

   **Note: Filename structure can obtain any text string placed into Item 3. The filename should be structured as follows:

   *[Filename]XXXXX.tif*

   Where X is equal to numbers listed in Items 4 and 5. In the event the number does not contain 5 digits, pad the number as follows:

   Example. *pyr-567-image00001.tif*

4. **First Image;** Input the first image from a set of LIF experiments.

5. **Last Image;** Input the last image from a set of LIF experiments.

6. **Number of Images to Skip;** Enter the number of images to skip in the experimental set. Using a Computer with 528 mb RAM this author could only capture 500 images to create a LIF or Intensity plot movie before encountering "out of memory" problems in MatLab.

7. **Frames Per Second;** Enter here the frame rate at which to record the movie, (typical 30).

8. **Intensity Low;** Enter here the low value in which to set the y axis of the intensity plot.

9. **Intensity High;** Enter here the High value in which to set the y axis of the intensity plot.

   **Note: Setting the values in Items 8 and 9 allow the user to focus between a particular intensity range to highlight a region of interest.

10. **Make Movie;** Function to initiate the movie making process based on input parameters.

    **Note: All images to be used in the making of an LIF or Intensity plot Movie must be copied into the following directory.

    *e:\george\matlab\movies*

11. **LIF Movie;** Function to play the recorded LIF movie in the MatLab environment.

    **Note: Playing movies in MatLab should be restricted to small image sets (200 images or less), larger image sets can be viewed better using a standard mpg media player.

12. **Intensity Movie;** Function to play the recorded LIF Intensity plot movie in the MatLab environment.

13. **Close;** Pressing this button closes the program and returns to the associated face seal directory of *e:\george\matlab.*

14. **Remove Dark Current;** Select this option when dark current from a digital camera is to be removed from a experimental data set. If dark current has been measured in the form of an image it must have the following filename.

    *darkcurrent.tif*

15. **Ave Intensity;** Select this option when it is desirable to obtain a plot of what the average intensity value is for each image in the experimental set. This provides a qualitative description of the behavior of the average minimum film thickness of the LIF experiment.

16. **LIF Movie;** Select this option when a LIF movie is desired to be recorded.

17. **Intensity Plot;** Select this option when a Intensity plot movie is desired to be recorded.

18. **Mirror Image;** Produce a left to right flip (mirror) of every image in the experimental data set.

19. **Colormap;** Changes the associated color scheme of the image to be processed.

*Reynolds.m* allows the user to perform theoretical hydrodynamic analysis for a 2-D surface wave. Analysis presented in Chapters 2 & 4 were performed using *Reynolds.m*

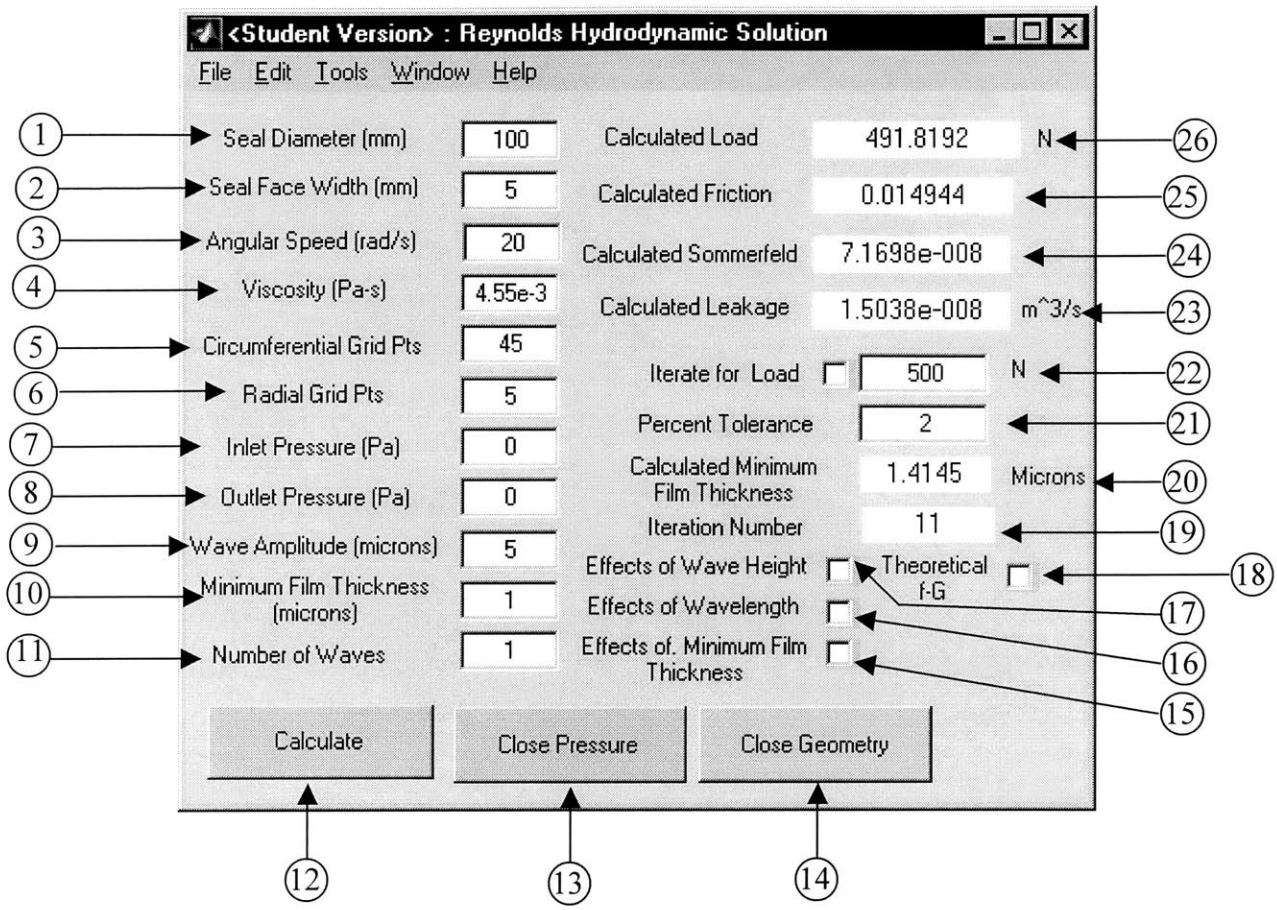


Programs called by *Reynolds.m*

*Reynolds.mat*
*Hydrodynamic.m*
*IterateHydrodynamic.m*
*LMFHydrodynamic.m*
*LWHydrodynamic.m*
*LWIHydrodynamic.m*

Numbered Explanation of Program *Reynolds.m*

1. **Seal Diameter;** Enter the diameter of the seal in mm.

2. **Seal Face Width;** Enter the face seal surface wave amplitude in microns.

3. **Angular Speed;** Enter the desired angular speed in rad/s.

4. **Viscosity;** Enter the viscosity of the lubricant in Pa-s.

5. **Circumferential Grid Points;** Enter the desired number of grid points to use in the circumferential direction.

6. **Radial Grid Points;** Enter the desired number of grid points to use in the radial direction.

7. **Inlet Pressure;** Enter the radial inlet pressure boundary condition (Pa).

8. **Outlet Pressure;** Enter the radial outlet pressure boundary condition (Pa).

9. **Wave Amplitude;** Enter the face seal surface wave amplitude in microns.

10. **Minimum Film Thickness;** Enter the desired minimum film thickness to be used for the analysis.

11. **Number of Waves;** Enter the number of surface waves to be used for the analysis.

12. **Calculate ;** Perform a hydrodynamic face seal analysis based on input parameters.

13. **Close Pressure;** Pressing this button closes the window with which contains the Reynolds pressure distribution.

14. **Close Geometry;** Pressing this button closes the window with which contains the plot of the face seal geometry.

15. **Effects of Minimum Film Thickness;** Selecting this option will perform an hydrodynamic analysis where the minimum film thickness is change form zero to the value in Item 10 in .05 micron increments.

    **Note: When this option is selected the program uses *LMFHydrodynamic.m* to perform the hydrodynamic analysis.

16. **Effects of Wavelength;** Selecting this option will perform an hydrodynamic analysis where the Wavelength is change form 1 to the value in Item 11 in 1 wave increments.

    **Note: When this option is selected the program uses *LWIHydrodynamic.m* to perform the hydrodynamic analysis. As the number of waves increases the resolution of the mesh becomes worse. For larger number of waves up to 15 the grid points should be increased to 320 for Item 5 and 25 for Item 6. This produces and m by n of 8000 points which is the limiting factor when using Matlab.

17. **Effects of Wave Height;** Selecting this option will perform an hydrodynamic analysis where the wave height is change form zero to the value in Item 9 in .5 micron increments.

    **Note: When this option is selected the program uses *LWHydrodynamic.m* to perform the hydrodynamic analysis.

18. **Theoretical f-G;** Selecting this option will create a coefficient of friction versus Sommerfeld plot described in Chapter 4.2 of this thesis. This requires a value of Load in Item 22.

    **Note: When this option is selected the program uses *fGHydrodynamic.m* to perform the hydrodynamic analysis.

19. **Iteration Number;** Relays to the user what iteration the program is performing.

20. **Calculated Minimum Film Thickness;** The value of minimum film thickness for iteration analysis is updated here.

21. **Percent Tolerance;** Enter the desired percent tolerance for load support.

22. **Iterate for Load;** Enter the desired load and select this option when it is desirable to iterate the load specified in this item. The solution will be within the percent tolerance of Item 21.

    **Note: When this option is selected the program uses *IterateHydrodynamic.m* to perform the hydrodynamic analysis.

23. **Calculated Leakage;** The value of calculated leakage for iteration analysis is updated here.

24. **Calculated Sommerfeld;** The value of calculated Sommerfeld Number for iteration analysis is updated here.

25. **Calculated Friction;** The value of calculated coefficient of friction for iteration analysis is updated here.

26. **Calculated Load;** The value of calculated load for iteration analysis is updated here.

*PressureGap.m* allows the user to perform theoretical Surface Tension analysis presented in Chapters 2 .

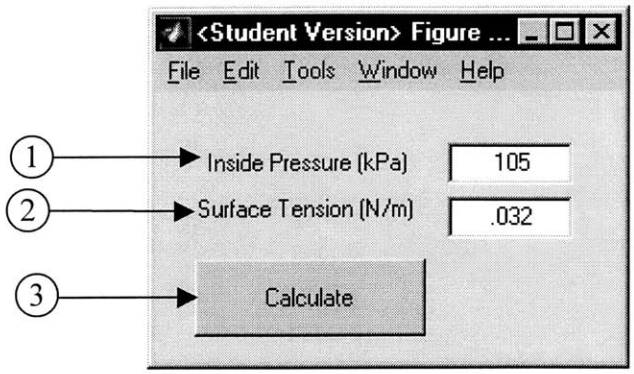


Programs called by *PressureGap.m*

*PressureGap.mat*
*SurfaceTension*

Numbered Explanation of Program *PressureGap.m*

1. **Inside Pressure;** Enter the desired inside pressure for the analysis in kPa.

2. **Surface Tension;** Enter the desired surface tension coefficient for the analysis in N/m.

3. **Calculate;** Function to calculate the plots similar to that of Figure 22. of Chapter 2.3.

**Appendix B**

# Dyed Oil Preparation for Laser Induced Fluorescence Experiments

Assuming Desired Dye Concentration is $8x10^{-4}$ mol Pyromethane 567nm /Liter Oil

*Chemicals:*

Pyromethane 567nm 6g (XXXX)
Dichloromethane ($CH_2Cl_2$)
Pennzoil 10w-30 Motor Oil

*Equipment:*

Lab Balance (mg scale)
Fume Hood with Closing Door and Exhaust
Hot Plate with Stirrer

(1) 100 mL beaker
(1) 1500 mL beaker
(1) metal spatula or small scoop
(1) thermometer (to 100 C)
(1) 1 L glass bottle with caps

Latex Gloves
Rubber Gloves
Chemical Splash Safety Goggles
Protective Apron

(1) piece of lab measuring paper
(1) stirring rod
(1) magnetic stirrer
(3) labels

*Procedure:*

1) Read all appropriate Material Safety Data Sheets and Equipment Operating Procedures.

2) In the fume hood, pour approximately 50 mL of $CH_2Cl_2$ into 100 mL beaker.

3) Measure exactly 0.362 g Pyromethane 567nm 6g onto lab measuring paper and gradually pour into beaker of $CH_2Cl_2$.

4) Stir the solution until the Pyromethane 567nm has dissolved (less than one minute).

5) Pour 0.946 L of Pennzoil 10w-30 (1 quart) into 1500 mL beaker.

6) Add $CH_2Cl_2$/ Pyromethane 567nm solution to oil. Stir until miscibility is observed (less than one minute).

7) Still in the fume hood, place the oil/solvent/dye mixture on hot plate with magnetic stirrer. Set stirrer to med-high to high speed (approx.. setting 8). Set temperature to low setting (approx.. setting 2). To quickly volatize the $CH_2Cl_2$, temperature should be above 40°C. DO NOT EXCEED 100°C. Continue until all $CH_2Cl_2$ has evaporated (check this by the level of mixture in the beaker -- level will be at approx. 950 L when complete). NOTE: As the $CH_2Cl_2$ volatizes, bubbles form and the volume increases. Temperature must return to 22°C to check whether evaporation is complete. Complete volatization at 65°C takes more than 3 hours, but not more than 20 hours (after 20 hours, oil will be maroon with a gold colored sheen - likely due to agglomeration of zinc anti-wear additives).

8) Clean up. Store dyed oil in glass bottle with cap and label appropriately. Dispose of all Pyromethane 567nm and $CH_2Cl_2$ as HAZARDOUS WASTE.